An Arctic Hurricane over the Bering Sea

STEVEN BUSINGER AND JONG-JIN BAIK

Department of Marine, Earth, and Atmospheric Sciences, North Carolina State University, Raleigh, North Carolina

(Manuscript received 29 August 1990, in final form 18 March 1991)

ABSTRACT

A mesoscale "arctic hurricane" developed over the western Bering Sea on 7 March 1977 and traveled eastward parallel to the ice edge along a zone of large sea surface temperature gradient. Satellite imagery reveals spiral cloud bands of unusual symmetry and mesoscale dimension associated with the mature stage of the low. The track of the low pressure center passed over the rawinsonde station at St. Paul Island where time series of surface data show a pronounced maximum in equivalent potential temperature at the core of the low. The storm made landfall with surface winds > 30 m s^{-1} at Cape Newenham, Alaska, on 9 March and rapidly dissipated thereafter.

Synoptic analyses show that the arctic hurricane formed at the leading edge of an outflow of arctic air that originated over the ice and passed over the open water of the western Bering Sea. In the mid- and upper troposphere a large cold-core low dominated the Bering Sea region. Quasi-geostrophic analysis at 0000 UTC 7 March 1977 reveals conditions conducive to synoptic-scale ascent over the region of the incipient low, as a sharp upper-level short wave crosses the Siberian coast. Conversely, during its mature stage little quasi-geostrophic forcing is seen over the low.

In order to investigate the ability of sea surface heat fluxes to develop and maintain the arctic hurricane, an analytical model based on the Carnot cycle, and an axisymmetric numerical model with the Kuo cumulus parameterization scheme are applied. The analytical calculation of the pressure drop from the outermost closed isobar to the storm center results in a central pressure of 973 mb, which agrees well with observation. When the initial environment of the numerical model is set to be similar to that observed with the arctic hurricane, the model correctly predicts the minimum sea-level pressure, strength of the wind circulation, and the magnitude of sensible heat fluxes observed with the storm. The dynamic and thermodynamic structures of the simulated storm are similar to those of tropical cyclones. The predicted development time of the storm is longer than observations suggest, and the diameter of the simulated anvil outflow is somewhat larger, pointing to the likely importance of baroclinic processes in the evolution of the disturbance, and the need for further numerical studies with mesoscale models that employ full three-dimensional primitive equations.

1. Introduction

In early March 1977 polar-orbiting satellite imagery witnessed the development of an unusually symmetric spiral cloud signature (Figs. 1b,c) from an incipient cloud band that was comma shaped (Fig. 1a). Closer inspection of the satellite imagery (Figs. 1b,c) reveals a cloud shield < 300 km in diameter and a clear "eye," reminiscent of a tropical cyclone. Fortunately, the storm center passed over the National Weather Service (NWS) rawinsonde station at St. Paul Island (57.3°N, 170.2°W; see Fig. 1c) in the Pribilof Islands. Time-series data from St. Paul Island reveal a sharp "V" in the surface pressure trace (Fig. 2), marking the passage of the low on 8 March 1977. By contrast, the temperature and dewpoint temperature traces evince pronounced maxima in equivalent potential temperature at the core of the disturbance (Figs. 2a,b). This finding is consistent with previous observational studies that

have found evidence of a warm core in some polar lows (e.g., Rasmussen 1981, 1983, 1989; Rasmussen and Zick 1987; Shapiro et al. 1987). An estimate of the diameter of the disturbance of ∼230 km (Fig. 2a) was obtained by making a time to distance conversion, using a storm propagation speed of ∼9.5 m s^{-1} (calculated from surface analyses and satellite imagery) and the time series of sea-level pressure data. The two-day path of the storm along the ice edge in the Bering Sea and its passage across St. Paul Island provide a favorable opportunity to investigate the environmental conditions associated with this unusual mesoscale cyclogenesis.

The characteristics of polar lows have been compared with tropical cyclones both in their observed structures (e.g., Rasmussen 1983, 1989) and dynamical aspects (e.g., Emanuel and Rotunno 1989, hereafter ER). Bergeron (1954) used the term "extratropical hurricane" in reference to cyclogenesis in old occluded cyclones as they passed over relatively warm water. Spiral-shaped cloud patterns of convective character have been observed to flare up within the inner cores of cold lows, without any obvious association with baroclinic features. The observed characteristics of these storms

―――――――

Corresponding author address: Dr. Steven Businger, Department of Marine, Earth, and Atmospheric Sciences, North Carolina State University, Raleigh, NC 27695.
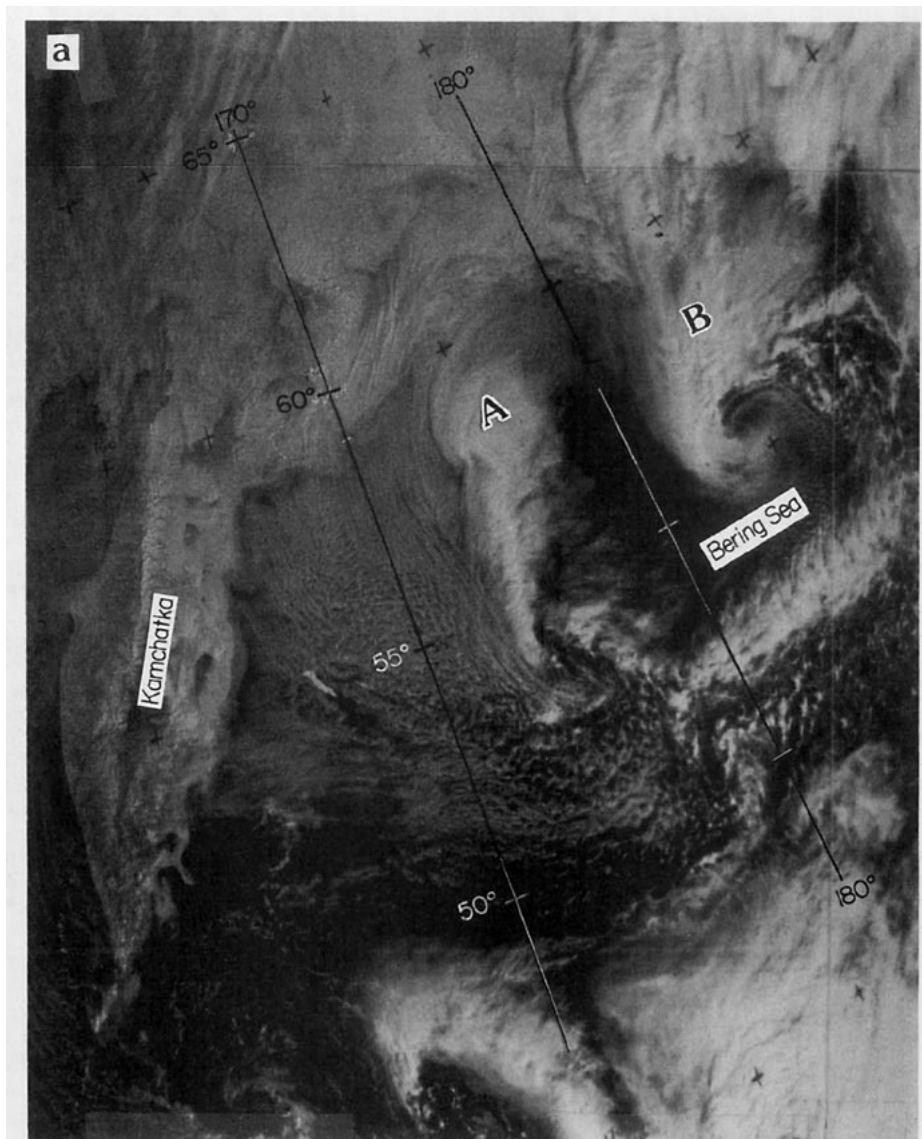
FIG. 1. Series of *NOAA-5* infrared satellite photographs of a polar low and cloud streets over the Bering Sea: (a) at 2230 UTC 6 March 1977. The letter "A" indicates the incipient comma cloud and "B" a cloud spiral associated with a dissipating occlusion, (b) at 2145 UTC 7 March 1977, and (c) at 2100 UTC 8 March 1977. The location of the NWS observing station at St. Paul Island is indicated by the small circled dot just to the west of the storm.

include very symmetric cloud signatures in satellite imagery, vigorous cumulonimbus surrounding a clear "eye," and a band of strong winds maximizing at low levels close to the core (Ernst and Matson 1983; Rasmussen and Zick 1987).

Several instability mechanisms have been proposed to explain cyclogenesis in cold airstreams over relatively warm oceans. In a study using mesoscale radar data, Harrold and Browning (1969) argued that baroclinic instability is the primary factor in polar-low development and many other studies (e.g., Mansfield 1974; Reed 1979; Reed and Duncan 1987; Moore and Peltier 1989) have supported this idea. On the other hand, a number of studies (e.g., Økland 1977, 1987; Rasmussen 1979; Bratseth 1985) have emphasized the role of conditional instability of the second kind (CISK). However, the CISK concept (Charney and Eliassen 1964) has been recently challenged by Emanuel (1986) in the theoretical study of tropical cyclone maintenance. His view against CISK arose from the observational evidence (Betts 1982) that the tropical atmosphere is nearly neutral to deep moist convection. Accordingly, in the tropical atmosphere there is little reservoir of available potential energy assumed by the original CISK theory. Using an axisymmetric tropical cyclone model with cumulus convection explicitly re-
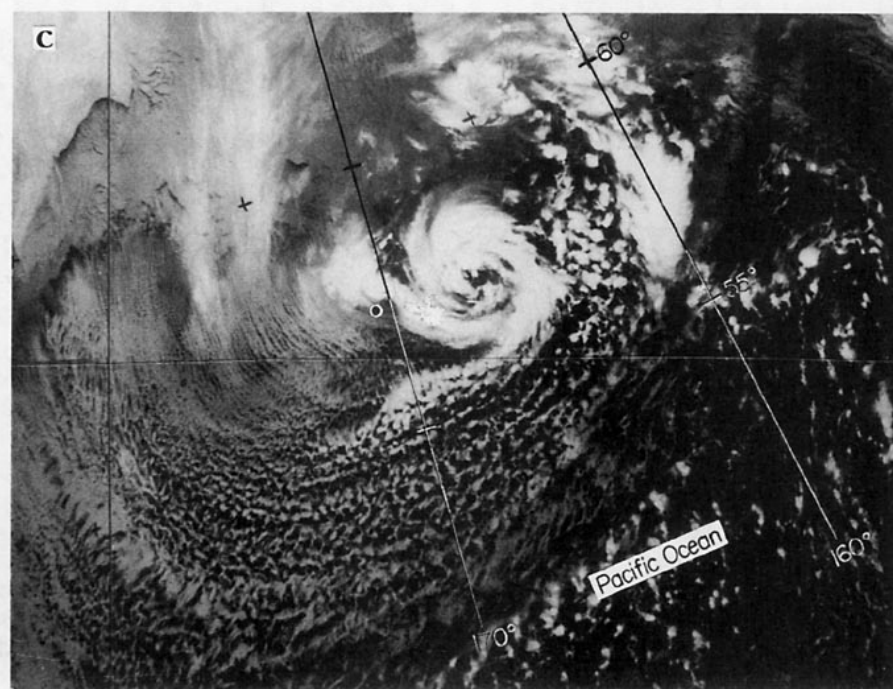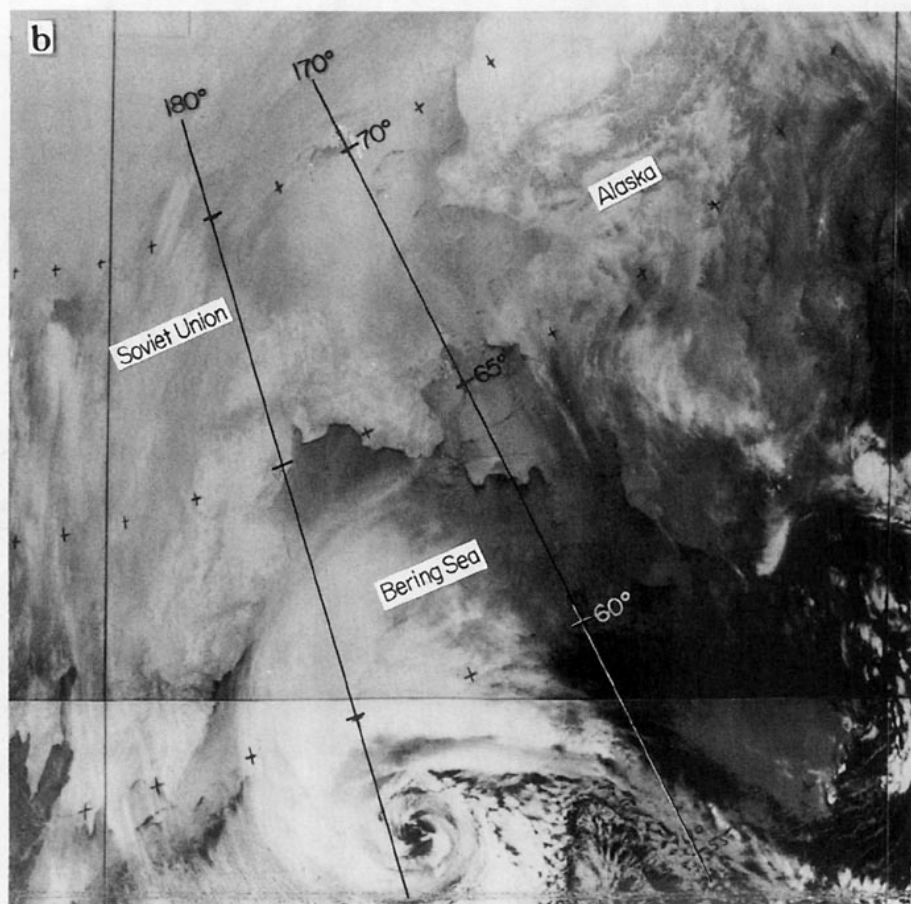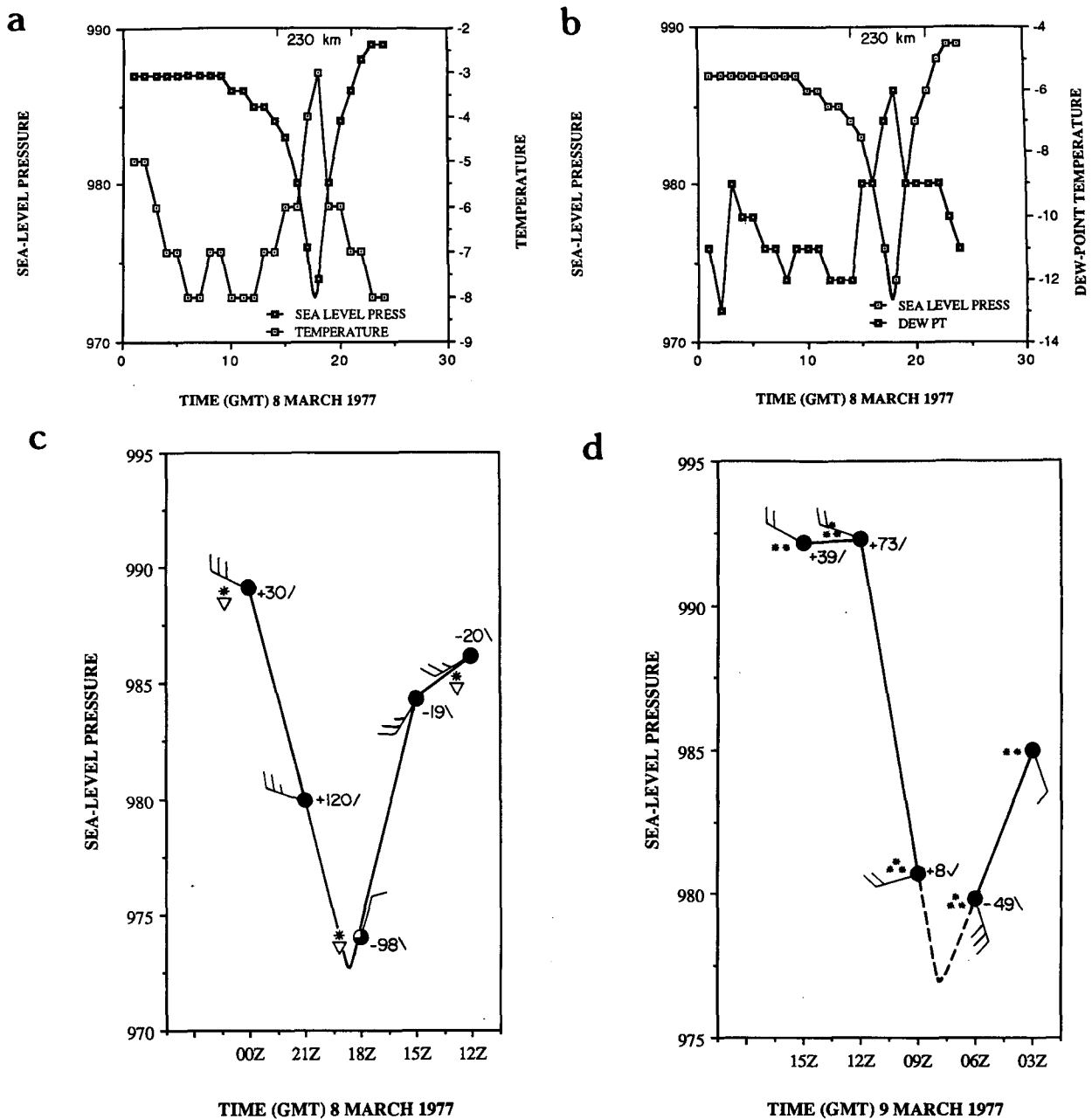
FIG. 1. (*Continued*)

FIG. 2. Hourly NWS data from St. Paul Island on 8 March 1977: (a) sea-level pressure (mb) and temperature (°C), (b) sea-level pressure and dewpoint temperature (°C), (c) sea-level pressure, current weather, 10-m winds (barb = 5 m s^{-1}) and surface pressure tendency $\{[\text{mb} (3 \text{ h})^{-1}] \times 10^{-1}\}$, (d) sea-level pressure, current weather, 10-m winds and surface pressure tendency at Cape Newenham, Alaska, on 9 March 1977 (58°N, 162°W).

solved, Rotunno and Emanuel (1987) showed that an organized initial vortex with sufficient amplitude, hence, convergence of anomalous sea surface fluxes, is needed for the vortex to intensify by air–sea interaction and the actual addition of energy from the ocean surface drives the storm. This view, called the air–sea interaction instability, has also been applied to account for the development of polar lows (ER).

Businger and Reed (1989a) differentiated three types

of polar-low development based on the degree of baroclinicity, static stability, and surface energy fluxes. These are short-wave/jet-streak type, arctic-front type, and cold-low type. Some polar lows are observed to develop as a combination of these types (e.g., Shapiro et al. 1987). When an upper-level cold low traverses the ice edge, it is possible for a complex storm system to develop that combines features of hurricane-like symmetry in a baroclinic environment. The relative

importance of baroclinicity and CISK or air–sea interaction instability, therefore, varies from case to case. For a general review of the subject of cyclogenesis in polar air masses, the reader is referred to Businger and Reed (1989b).

The first objective of this research is to document the synoptic environment during the incipient and mature stages of the polar low (sections 2 and 3). Differences between these environments may have im-

plications regarding the physical mechanisms that are important in the genesis of the disturbance, and those that are active in sustaining the storm during its extended mature stage. In section 4 the influence of surface sensible and latent heat fluxes is discussed. The second objective of this study is to investigate the ability of air–sea interaction instability to develop and sustain the arctic storm (section 5). For this purpose, an axisymmetric numerical model with parameterized con-
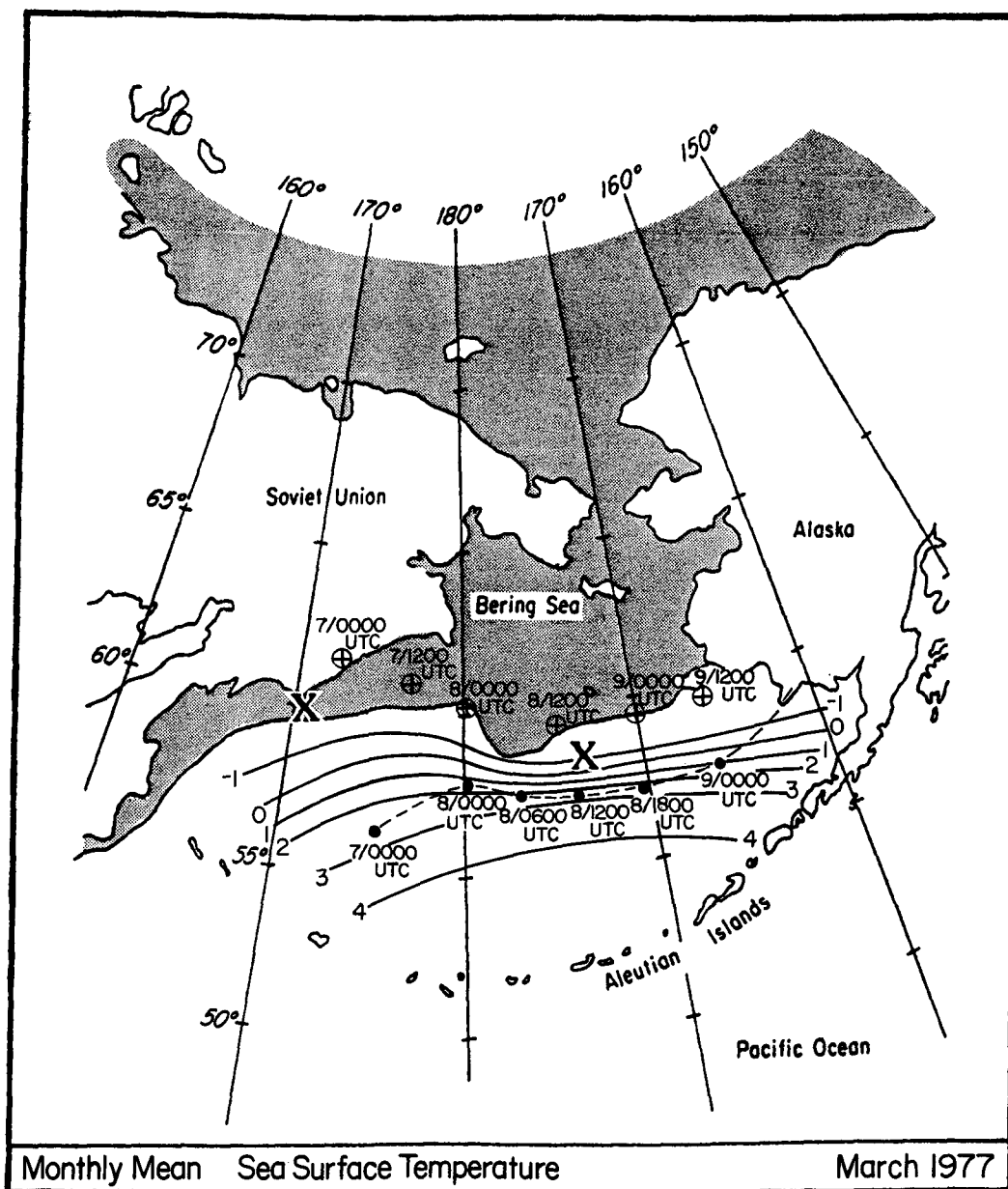

FIG. 3. Monthly mean sea surface temperature (°C) and extent of the ice (shaded region) for March 1977 in the Bering Sea (after Ingraham 1983). Positions of the center of the 500-mb cold-core low are indicated by the circled crosses, with the date and time (UTC) shown. The position of the centers of maximum positive vorticity at 500 mb for 0000 UTC 7 March, and 1200 UTC 8 March are shown by "X." The thin dashed line shows the track of the surface low pressure center.

vective processes is used. The use of axisymmetric geometry eliminates baroclinic forcing to the polar-low development and enables us to study the role of air–sea interaction instability in the storm evolution.

The unusual symmetry displayed by the storm's cloud shield in its long path across the Bering Sea, its warm, high-θ_e core, and the success of the numerical model in simulating major features of the storm led to adoption of the term *arctic hurricane* in this study. This term has been used previously by ER. In this paper, an arctic hurricane is defined as a polar low with symmetric signature (e.g., Businger and Reed 1989b) and threshold winds ≥ 25 m s^{-1}, in which surface fluxes play the dominant role in the structure and sustenance of the mature storm.

2. Synoptic analysis

To provide the best possible synoptic documentation of this event, a diagnostic approach is used in which all horizontal maps presented in this paper are reanalyzed, incorporating all available data from the National Climatic Data Center (NCDC) and satellite imagery from the National Environmental Satellite Data and Information Service (NESDIS) (R. K. Anderson, personal communication). The geographical setting, location of the ice edge, and monthly mean sea surface temperatures in the Bering Sea for March 1977 are shown in Fig. 3. Also shown in Fig. 3 are the track of the low pressure center at the surface, the positions of the 500-mb cold-core low center, and the center of maximum positive vorticity at 500 mb. Vorticity was calculated using the Barnes objective analysis scheme (see the Appendix). Each track parallels the ice edge, with the surface track following the axis of strongest sea surface temperature gradient, an observation that has been made in cases of rapid cyclogenesis (e.g., Bosart 1981).

The genesis of the arctic hurricane can be traced to 0000 UTC 7 March (Fig. 4). The surface analysis (Fig. 4a) shows a trough of low pressure extending east–west across the Bering Sea south of the ice edge. The data coverage, including upper-air observations, over the Bering Sea region of this case study is relatively good, despite the remote high-latitude location. However, a void in the data distribution in the vicinity of the incipient low at this time illustrates a difficulty that the small scale of polar lows often presents operational and research meteorologists. Although the exact location of the low center and details of the stage of development of the storm cannot be resolved at this time, the larger synoptic environment, including the likely general location of a low south of the ice edge, can be inferred from the surrounding surface data, satellite imagery, and time continuity. A packing of the isobars to the west of the incipient surface-low center (984 mb) over the western Bering Sea results in pronounced cold-air advection, as unmodified arctic air passes southward

over open water. A temperature gradient of $>10°C$ $(200\text{ km})^{-1}$ can be seen over the western Bering Sea at this time. Satellite imagery for 2230 UTC 6 March (Fig. 1a) shows longitudinal convective roll vortices (Kuettner 1959; LeMone 1973) or cloud streets, indicative of boundary-layer modification by surface fluxes of latent and sensible heat. The orientation of the cloud streets can be related to the mean wind component in the boundary layer (Brown 1980). Recent observations taken by research aircraft have shown that the modification of arctic boundary-layer air by surface fluxes can produce zones of strong low-level baroclinicity, and low Richardson number (Businger and Walter 1988; Shapiro and Fedor 1989). These zones of contrast between modified and unmodified boundary-layer air are referred to as arctic fronts. A comma-shaped cloud band seen in the northeasterly flow north of the incipient low (984 mb in Fig. 4a) is probably the reflection of a disturbance that is forming along an axis of concentrated low-level baroclinicity. Data resolution does not allow the strength of the low-level baroclinicity to be resolved in the present case. Therefore, no attempt was made to analyze arctic front positions, despite the presence of significant baroclinicity in isotherm analyses in the lower troposphere over the Bering Sea in this study (Figs. 4–8). The spiral-shaped cloud signature visible to the east of the comma cloud (Fig. 1a) is associated with a low pressure center (980 mb in Fig. 4a) at the core of a dissipating parent occlusion. This low does not develop further as it tracks eastward with time.

Height and temperature analysis at the 850-mb level for 0000 UTC 7 March (Fig. 4b) shows a trough axis directly over the incipient low. Temperatures below $-30°C$ are observed along the southern coast of Siberia at this time, with cold advection indicated over the western Bering Sea. A westward tilt with height of the trough axis indicates the potential for baroclinic growth (Fig. 4c,d).

The stars plotted on figures showing upper-level geopotential analyses indicate data derived from the *NOAA-5* polar-orbiting satellite. These data are representative of a layer mean and are known to contain significant errors, with a tendency to overestimate the temperature and height. Consequently, these data were given secondary weight to the rawinsonde data in the analyses.

At 700 mb, the flow over the comma cloud is westerly (Fig. 4c) over a region in which the surface flow is northeasterly, as implied by the orientation of the cloud streets in Fig. 1a and the surface analysis (Fig. 4a). This indicates a reversal of wind direction with height. Such wind shear with height has been documented previously in cases observed over the Norwegian Sea in which a series of small polar lows form along an axis of concentrated low-level baroclinicity (Duncan 1977; Reed and Duncan 1987). In such cases, the storm motion (or wind at the steering level) is in
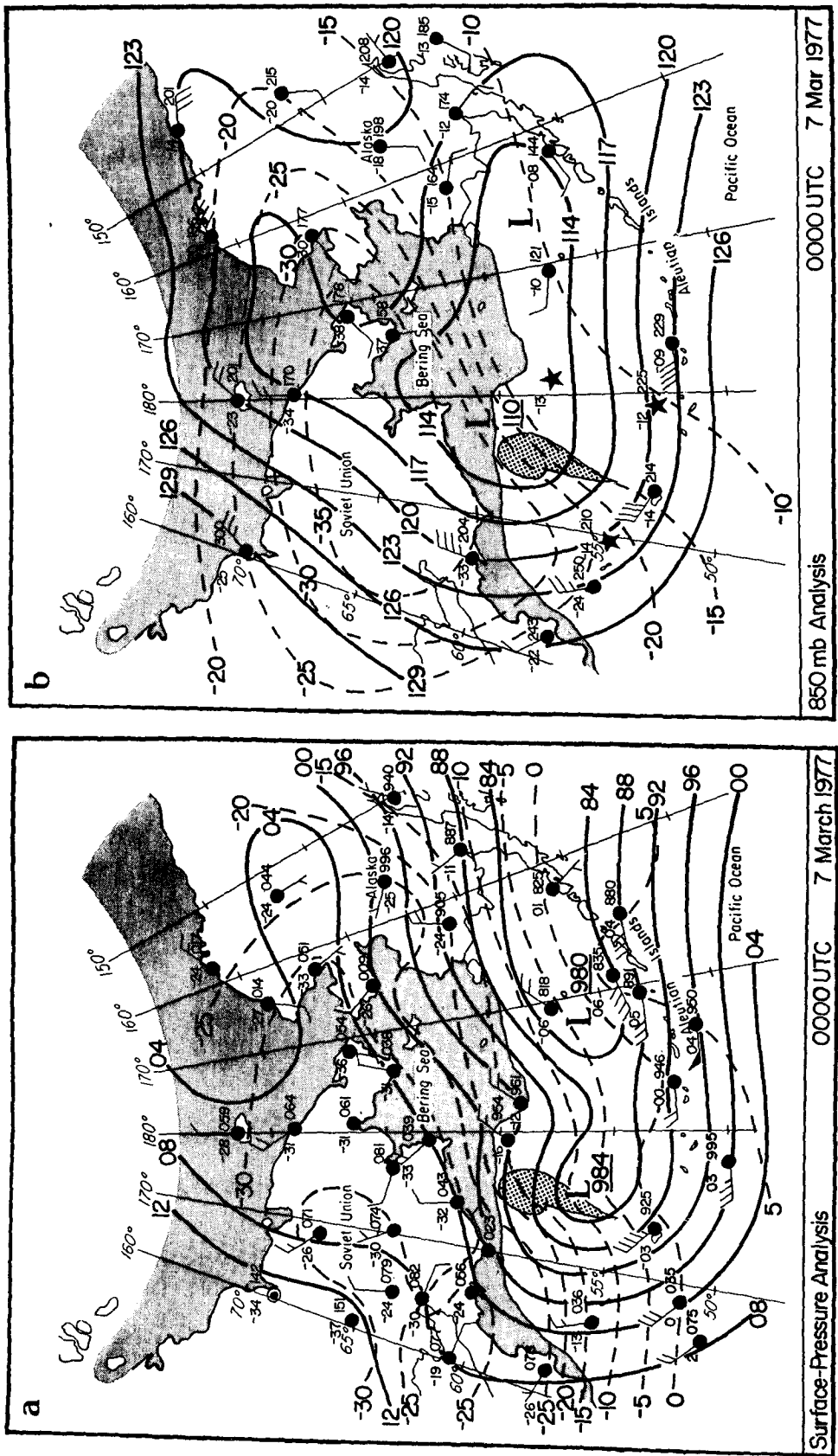
FIG. 4. Analyses for 0000 UTC 7 March 1977: (a) Surface-pressure analysis (solid contours are temperature every 5°C). Geopotential analysis (solid contours: height every 30 m, dashed contours: temperature every 5°C) for (b) 850 mb, (c) 700 mb, and (d) 500 mb (height every 60 m). The stars in (b), (c), and (d) indicate data derived from polar-orbiting satellite. The shaded region indicates the approximate extent of the ice cover, and coarse shaded areas indicate the approximate extent of the cloud cover derived from satellite imagery in Fig. 1a.
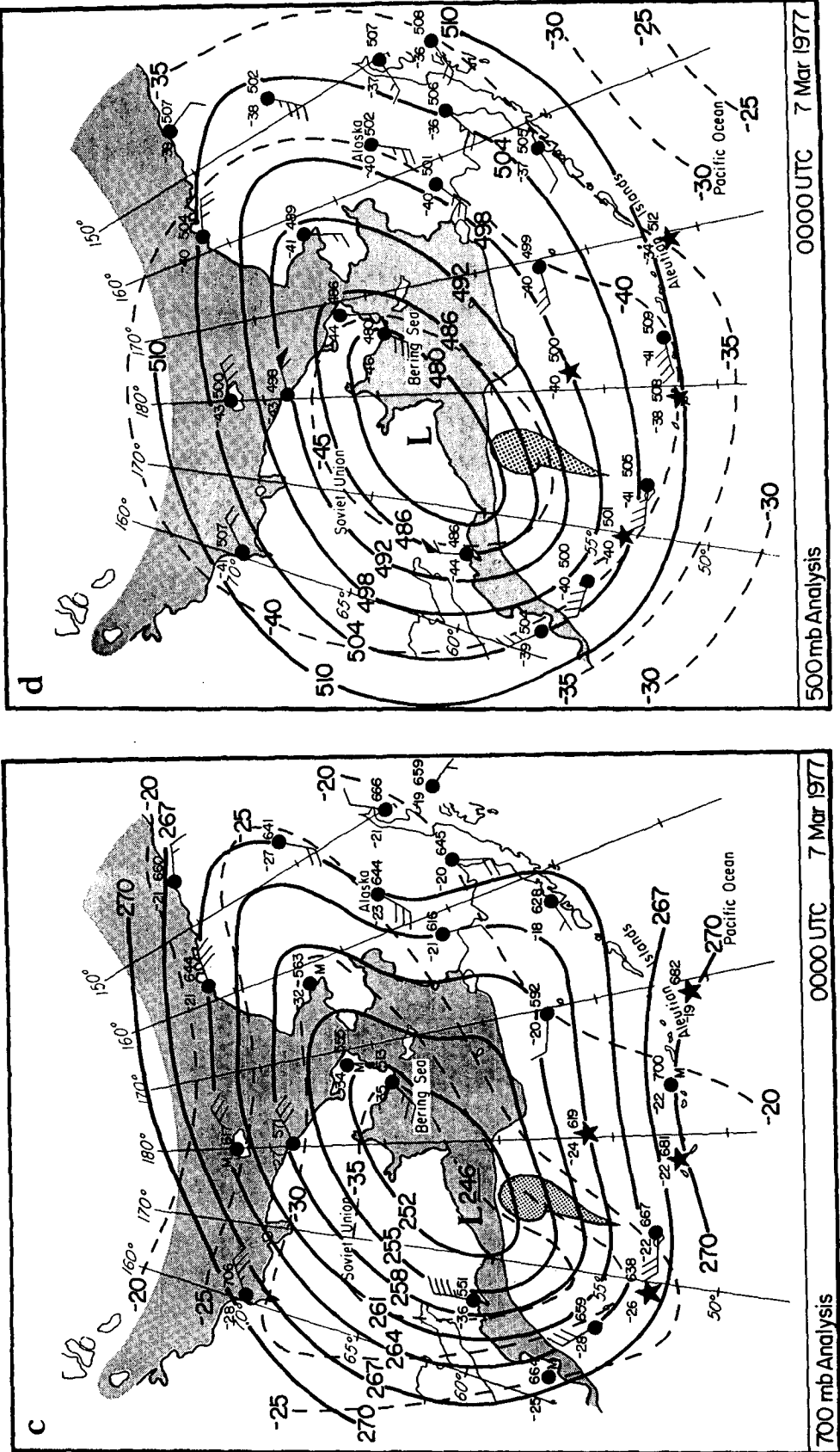
FIG. 4. (*Continued*)

a direction opposite to the thermal wind, leading to the term "reverse shear." Lin (1989) has used a quasigeostrophic theory of cyclogenesis to model the growth of a disturbance forced by an isolated low-level diabatic heat source in a backsheared baroclinic flow. A low is shown to be produced hydrostatically by less dense air above the heating region. Moore and Peltier (1989), in a study using a primitive numerical model, show that small-amplitude perturbations on a shallow baroclinic zone are highly unstable, with the fastest-growing disturbances exhibiting horizontal length scales on order of 500 km. Furthermore, they show that these disturbances display many features in common with the Norwegian cyclone model (Bjerknes and Solberg 1922), including the tendency to exist in cyclone families or wave trains. A limitation of their model, however, is the absence of friction.

The 500-mb height and temperature analysis at 0000 UTC 7 March (Fig. 4d) shows that a cold-core vortex (with temperatures $< -45°C$) dominates the Bering Sea region. A short-wave trough over the western Bering Sea provides conditions conducive to upward vertical motion (Holton 1979) over the region of the incipient low. This point will be explored further in section 3 of this paper.

A continued void in data distribution in the vicinity of the developing arctic hurricane is seen in the surface analysis for 1200 UTC 7 March 1977 (Fig. 5a). The presence of a low is again implied by the surrounding surface data, however, the stage of development of the storm cannot be resolved at this time.

Gradient-wind constraints and time continuity were used at the higher levels to elucidate the significant features of the atmospheric circulation aloft over the Bering Sea. At the 700-mb level (Fig. 5b) the cold-core low continues to dominate the Bering Sea with enhanced cyclonically curved flow located over the region of surface development in the western Bering Sea.

By 2145 UTC 7 March the satellite imagery shows a fully developed arctic hurricane (Fig. 1b), with cold convective clouds and an asymmetric distribution of outflow cirrus surrounding a cloud-free "eye." The diameter of the outflow cirrus is >600 km at this time. The surface analysis for 0000 UTC 8 March (Fig. 6a) shows that the low center is at the apex between low-level warm and cold advection. A ship located near the ice edge (58°N, 177°W) provides critical confirmation of the intensity of the surface circulation at this time. The 700-mb low center is to the north of the surface low center (Fig. 6b), placing the surface low on the cyclonic-shear side of the enhanced upper-level flow.

A well-defined low at 850 mb is observed just to the northwest of St. Paul Island at 1200 UTC 8 March (Fig. 7a), with cold advection indicated on its southwest side. The cold vortex aloft (Figs. 7b,c) is nearly collocated with the low at 850 mb. The observed 500-mb height has decreased to 487 dam and the temper-

ature has fallen to −46°C over St. Paul Island by this time.

Surface analyses on 8 March (Fig. 8) show that the arctic hurricane progressed eastward across the Bering Sea to St. Paul Island in phase with the upper-level vortex. At 0600 UTC (Fig. 8a) the surface low remains at the apex between low-level cold and warm advection as it tracks parallel to the ice edge. The surface low at 1200 UTC (Fig. 8b) is located just south of the upper-level low, again on the cyclonic-shear side of the enhanced flow aloft (Fig. 7). The strength of the surface low was difficult to document early on 8 March and is likely underestimated in Figs. 8a,b. By 1800 UTC the surface low had just passed St. Paul Island, with an estimated central pressure of ~970 mb (Fig. 8c). The striking spiral cloud pattern in the satellite image for 2100 UTC 8 March (Fig. 1c) bears witness to the unusual symmetric organization and continued potency of the arctic hurricane at this time. Cloud streets are observed on the northwest side of the low, indicative of enhanced outflow of arctic air in the wake of the storm.

The upper vortex crossed the west coast of Alaska just after 1200 UTC 9 March. Throughout the 60-h period from 0000 UTC 7 March to 1200 UTC 9 March, unusually cold temperatures and low heights were associated with the dominant upper-level vortex as it tracked eastward along the ice edge (Fig. 3).

After making landfall at Cape Newenham at ~0800 UTC 9 March, the arctic hurricane rapidly dissipated over the Alaskan subcontinent. This is illustrated in Fig. 9, which shows the change in minimum sea-level pressure with time from 7 March through 9 March. The values of the storm central pressure on 7 March and those for 0600 and 1200 UTC 8 March are of necessity only rough estimates based on the surface analyses presented earlier in this section and tend to underestimate the actual values. The proximity of surface observations to the storm center lends greater confidence to the central pressure estimates for 0000 UTC 8 March and for those after 1200 UTC 8 March. The most rapid filling of the low seen in Fig. 9 occurs just following its crossing of the Alaskan coast. Weakening of the surface circulation can be seen in the sea-level analysis for 1200 UTC on 9 March (Fig. 10a), despite the continued presence of significant low-level baroclinicity. Aloft the 700-mb analysis (Fig. 10b) still indicates a vigorous closed low with cold temperatures (−30°C observed at St. Paul Island). The weakening of the storm over land is promoted by the removal of the surface heat source and the additional dissipative impact of orography over western Alaska.

Rawinsonde soundings taken at 1200 UTC 7 March and 1200 UTC 8 March (Figs. 11a,b) just prior to the passage of the arctic hurricane show that marked cooling has taken place in the midtroposphere (from ~880 to 500 mb), and warming below ~880 mb during the intervening 24 h, with the latter sounding displaying
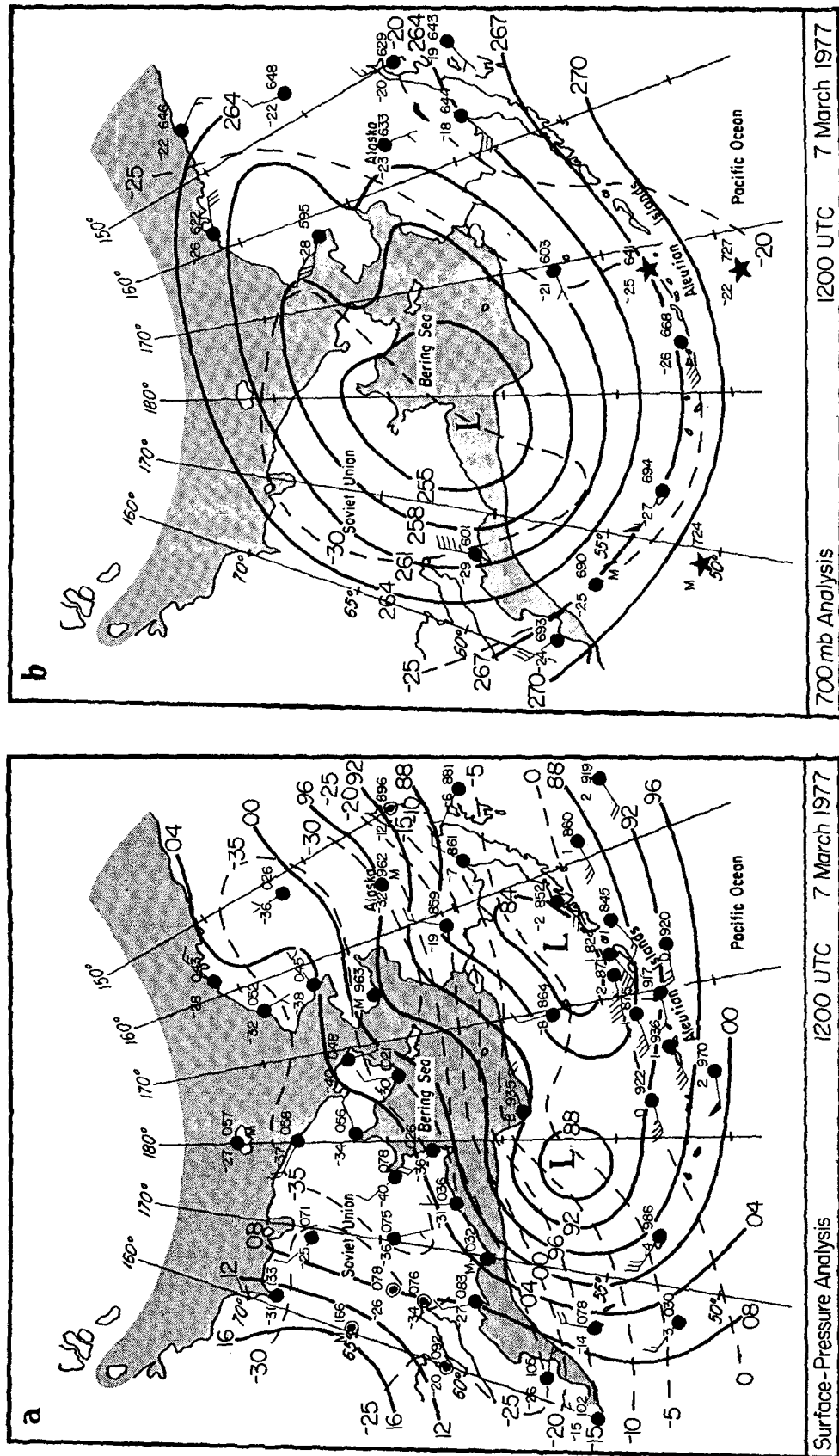
FIG. 5. As in Fig. 4, except for 1200 UTC 7 March 1977: (a) Surface-pressure analysis, (b) geopotential analysis for 700 mb.
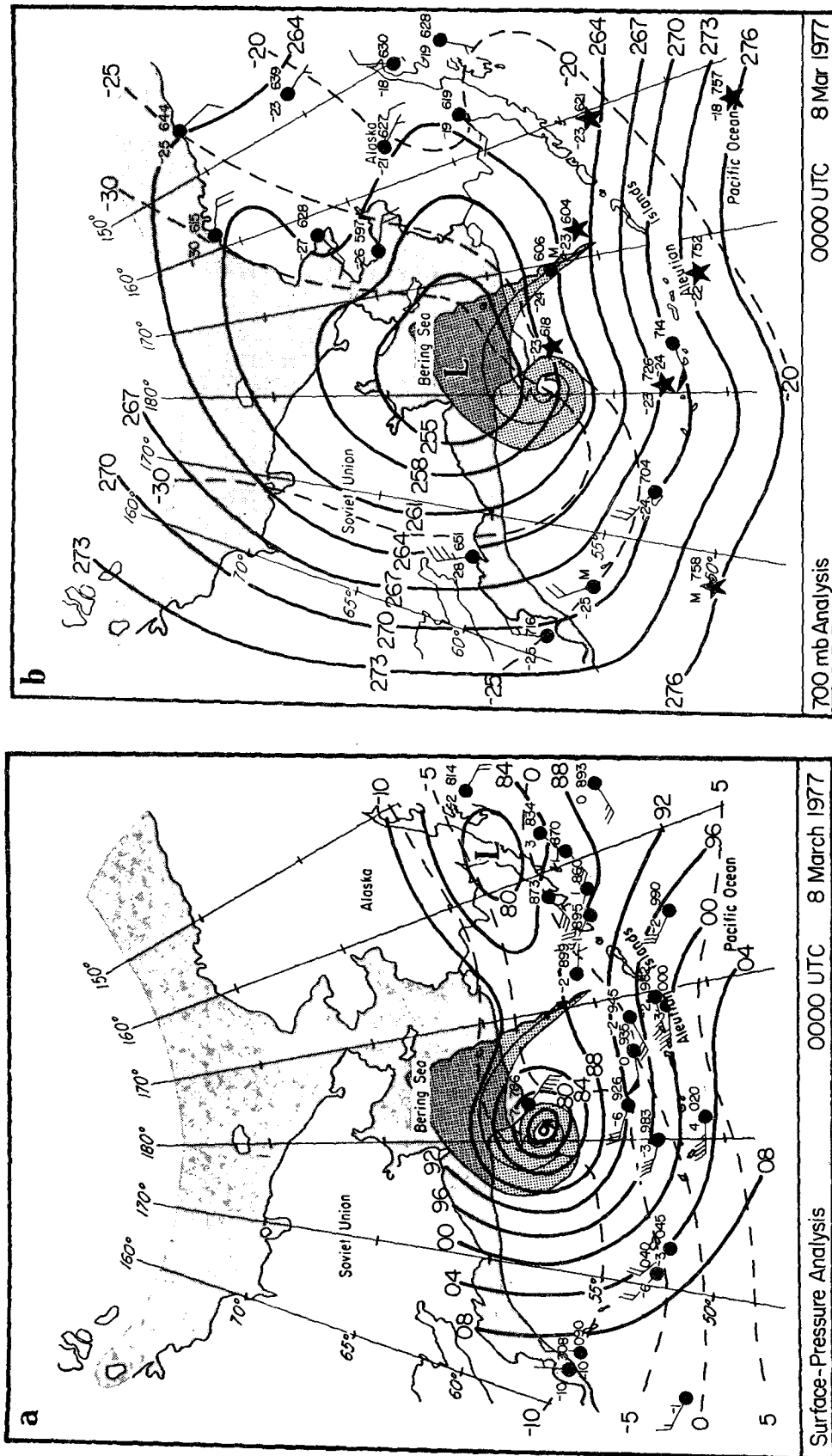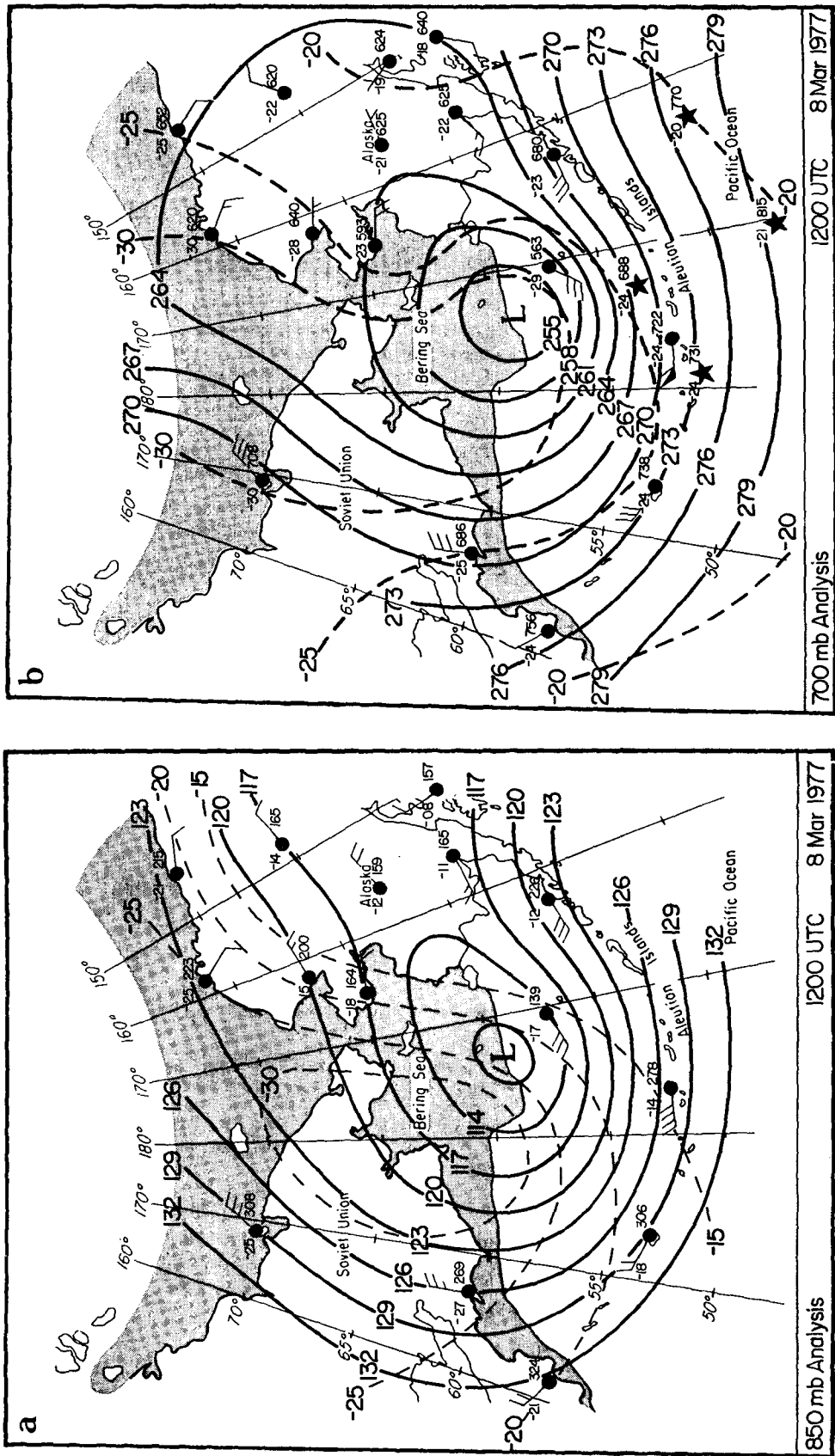
FIG. 6. As in Fig. 4, except for 0000 UTC 8 March 1977: (a) Surface-pressure analysis, (b) geopotential analysis for 700 mb. The coarse shaded areas indicate the approximate extent of the cloud cover derived from satellite imagery in Fig. 1b.
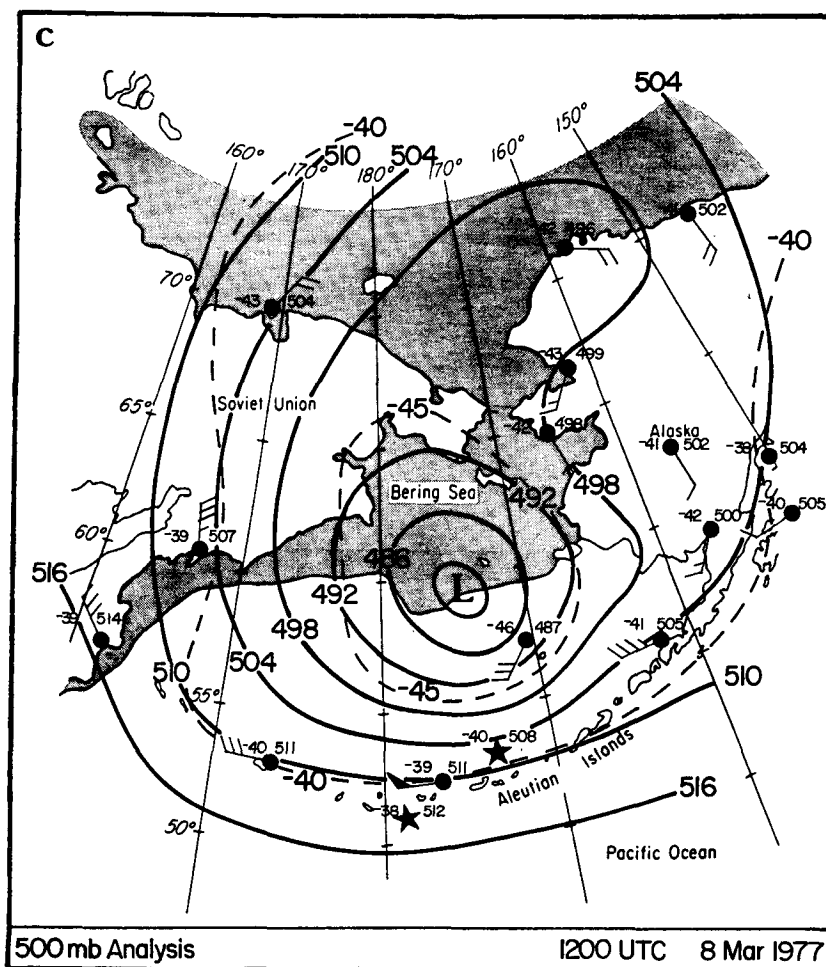
FIG. 7. Geopotential analyses for 1200 UTC 8 March 1977: (a) 850 mb (solid contours are height every 30 m, and dashed contours are temperature every 5°C), (b) 700 mb, and (c) 500 mb (height every 60 m).

FIG. 7. (*Continued*)

warmer dewpoint temperatures below ~720 mb. The soundings also reveal a very low tropopause height of <6 km. The magnitude of the cooling seen at St. Paul Island prior to the passage of the storm is evidence of the strong synoptic-scale cold advection with which the arctic hurricane was associated. A pronounced inversion at ~900 mb in the 7 March sounding marks the top of the arctic boundary layer (Fig. 11a). Such low-level inversions may be a ubiquitous feature of the environment in which arctic hurricanes form. Økland (1989) argues that surface heat fluxes confined to the shallow arctic boundary layer are transported towards low pressure by the Ekman layer flux, where the heat and moisture feed the deep convection. Økland cites the absence of the low-level inversions in maritime polar air masses in midlatitudes for the lack of arctic hurricanes observed in these regions.

3. Quasi-geostrophic analysis

Previous observational studies (Businger 1985 and 1987; Rasmussen 1985) have pointed to the presence

of a midtropospheric cold-core vortex that dominates the environment in which polar-low outbreaks occur. Mesoscale vorticity maxima in the midtroposphere that rotate about cold-core lows have also been documented (Zick 1983). Quasi-geostrophic analysis was undertaken to investigate the role of the midtropospheric short wave (Fig. 4d) in the genesis of the arctic hurricane in this case study.

A convenient method of viewing geostrophic forcing of vertical motion is divergence of the Q vector (Hoskins et al. 1978). The omega equation can be written:

$$\left(\sigma\nabla^2 + f_0{}^2 \frac{\partial^2}{\partial p^2}\right)\omega = -2\nabla\cdot\mathbf{Q}, \qquad (1)$$

where the x, y components of $\mathbf{Q}$ are given by:

$$\mathbf{Q} = \left[-\frac{R}{p}\frac{\partial\mathbf{V}_g}{\partial x}\cdot\nabla T_v, \ -\frac{R}{p}\frac{\partial\mathbf{V}_g}{\partial y}\cdot\nabla T_v\right]. \qquad (2)$$

Here ω is the vertical p velocity, p is the pressure, T_v is the virtual temperature, σ is the static stability parameter, f_0 is the Coriolis parameter at 61.5°N (mid-
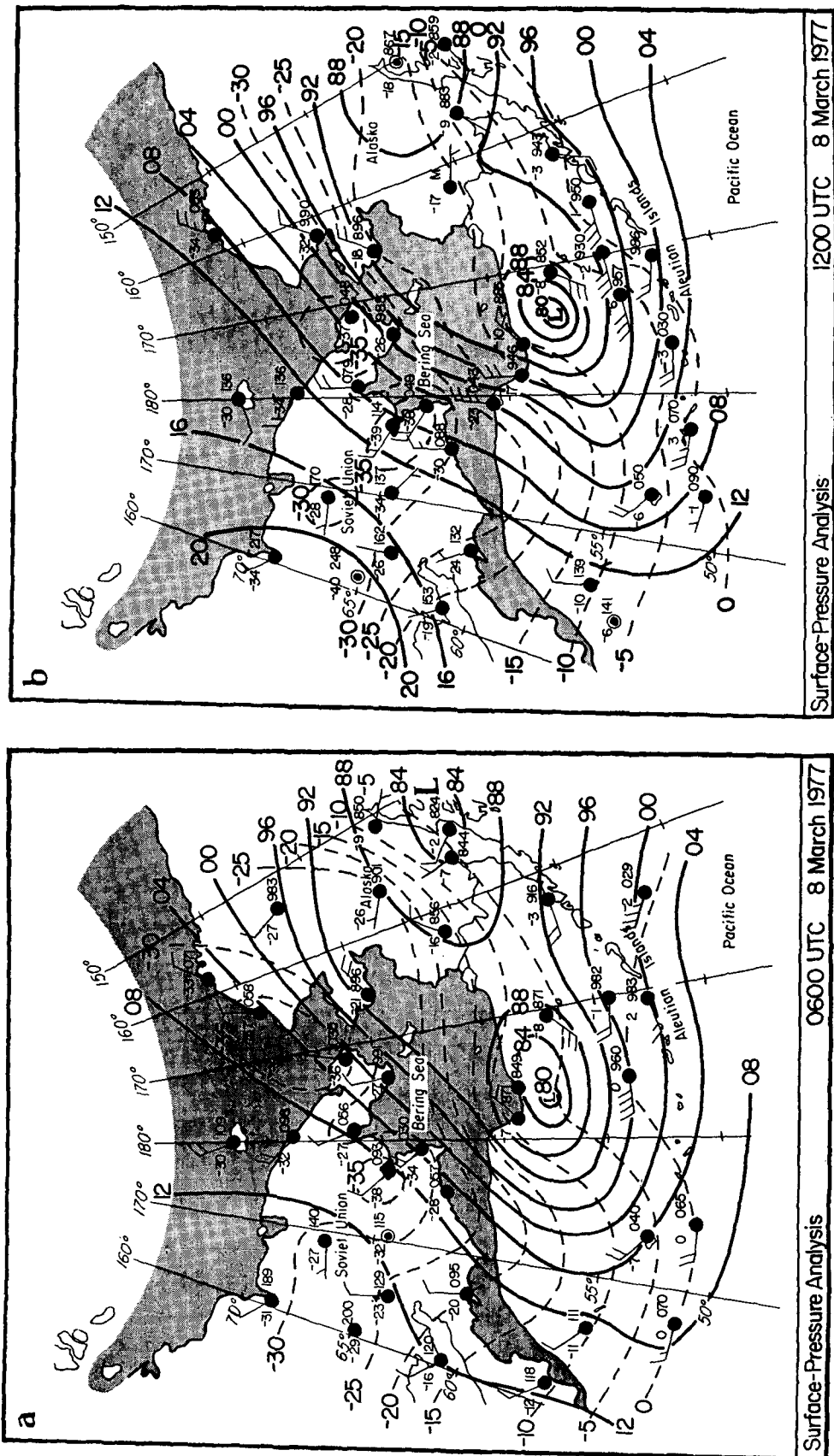
FIG. 8. Surface-pressure analyses (solid contours are isobars every 4 mb, dashed contours are temperature every 5°C) for: (a) 0600 UTC 8 March, (b) 1200 UTC 8 March, and (c) 1800 UTC 8 March.
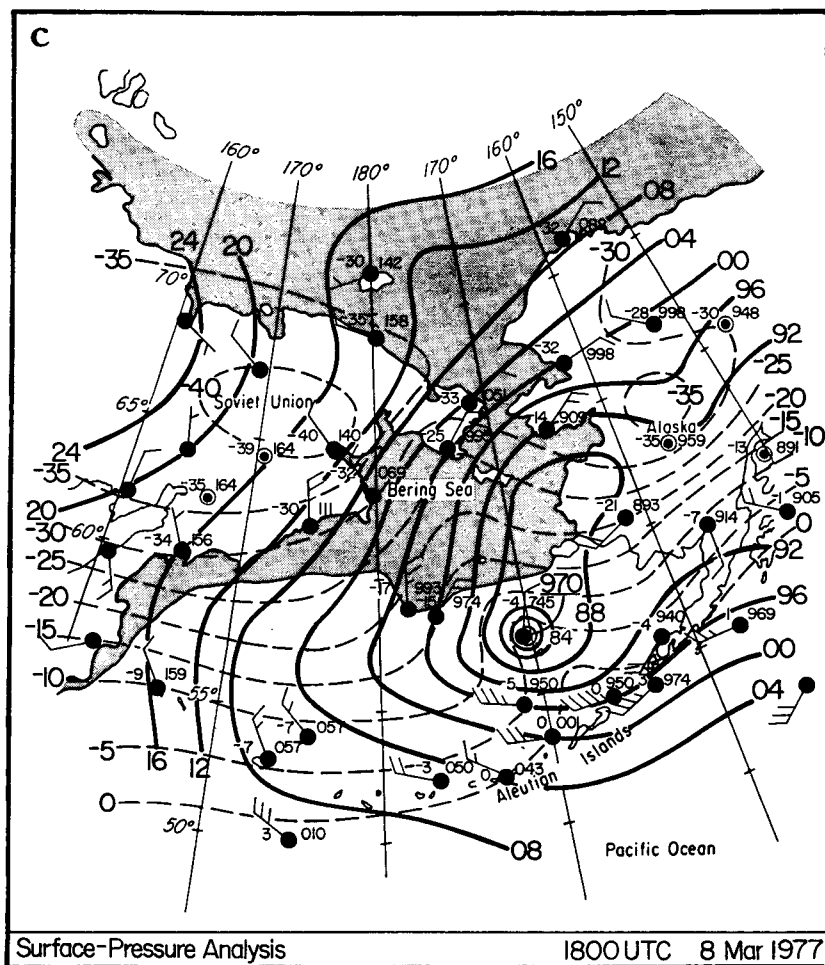
FIG. 8. (*Continued*)

point of the grid), V_g is the geostrophic wind vector, and R is the gas constant. The gradient and Laplacian operators are two-dimensional in x,y. The Q vector provides an approximate picture of the ageostrophic horizontal wind in the lower branch of the circulation that develops in order to maintain thermal-wind balance in an evolving synoptic disturbance (Hoskins and Pedder 1980). Convergence of the Q vector (positive forcing) implies ascending motion ($\omega < 0$), while divergence of Q (negative forcing) implies subsidence ($\omega > 0$). The Barnes objective analysis scheme provided gridded data for calculating the forcing ($-2\nabla \cdot Q$). For the details see the Appendix.

A three-dimensional relaxation of the forcing was then performed to obtain ω at three equally spaced levels (850, 700, and 550 mb) in the troposphere. The lateral and lower (1000 mb) boundary conditions on ω were set to zero. Soundings in the vicinity of the polar-low center (e.g., Fig. 11) show a tropopause below 400 mb, so the upper boundary condition on ω was set to zero at 400 mb. The sounding nearest the low center (Fig. 11b) suggests a static stability σ close to

the moist adiabatic, a choice used by Gyakum and Barker (1988) and also adopted here. The forcing pattern calculated for 500 mb was substituted at 550 mb, rather than performing a vertical interpolation necessary to obtain the nonstandard level. The approximations incorporated in the calculation of ω may lead to a slight overestimate of the vertical velocities. However, the broad pattern of the forcing and qualitative results for ω are correct and are what is of interest to the discussion that follows.

Figure 12 shows patterns of forcing ($-2\nabla \cdot Q$) and ω for 0000 UTC 7 March. In the mid- and upper troposphere (700 and 500 mb) forcing is strongly positive over the incipient comma cloud, and ω is negative indicating upward motion in the troposphere at this early stage (Figs. 12a,b). The greatest forcing for upward motion is at 500 mb and is centered over the head of the comma cloud in a region of positive vorticity advection (PVA) associated with the 500 mb short-wave trough. The maximum upward motion in this region is $\omega \sim -4$ μb s^{-1} at 550 mb, $\omega \sim -2$ μb s^{-1} at 700 mb, and $\omega \sim -1$ μb s^{-1} at 850 mb (see asterisks in
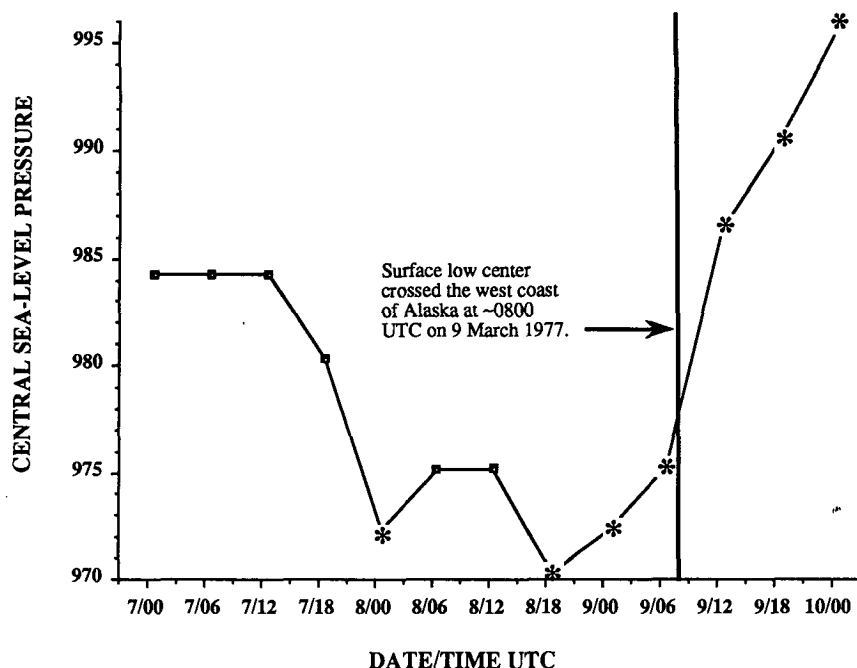
FIG. 9. Central (minimum) sea-level pressure analyzed in the arctic hurricane from 0000 UTC 7 March through 0000 UTC 10 March 1977. Asterisks indicate surface observations near the low center and increased confidence in the minimum pressure estimates.

Fig. 12). At 850 mb the convergence of Q is weakly negative (Fig. 12c), consistent with cold advection at this level (Fig. 4b). A region of positive ω associated with subsiding air is located east of the comma cloud, with the maximum descent at all three levels near ~60°N, 179°W. This result is in qualitative agreement with the satellite image taken just prior to this time (Fig. 1a), which shows a relatively cloud-free band along the date line.

Calculations of Q were also made for 1200 UTC 8 March (Fig. 13) when the arctic hurricane was well developed (Fig. 8b). At this time, values of forcing and ω are near zero over the surface-low center at all three levels (Fig. 13). At the 500-mb level (Fig. 13a), the surface low is located just south of the cold-low center, and almost directly under the positive vorticity maximum, in a region of small forcing. Areas of greater forcing are seen radially farther out from the center of the upper-level low. However, absolute values of ω are small over the entire domain, with a minimum value of ~ -1.5 μb s^{-1} over the Aleutian Islands, well to the southeast of the surface low. The convergence of Q is particularly weak at the 700-mb level (Fig. 13b), with an absence of forcing and very small ω in the vicinity of the mature surface low. At 850 mb, a dipole of upward and downward forcing is seen to the northwest of the surface low, primarily in response to thermal advection, but again no forcing is present over the mature surface low. The largest values of ω (~3 μb s^{-1}), associated with descent, are in a region of enhanced cold advection on the west side of the low.

In summary, during the incipient phase of the storm, an upper-level short-wave trough approaching the surface low results in quasi-geostrophic forcing and implied upward vertical motions ($\omega < 0$) over the incipient low. It is suggested that the initial development of the disturbance is induced by a cyclonic potential-vorticity anomaly in the upper troposphere, associated with the short-wave trough that acts on vorticity-rich air at low levels (Hoskins et al. 1985). During the mature phase, little or no quasi-geostrophic forcing is evident over the storm. At this time synoptic-scale descent is implied in the lower troposphere in a region of cold advection to the west of the low.

4. Sea surface fluxes

It has been argued that the potential warming of an air column in the core of a polar-low circulation, due to surface fluxes of sensible and latent heat, can account for observed deepening at the surface (e.g., Businger 1987). In this section, we explore the importance of the surface heat fluxes for the case presented in this paper.

A bulk aerodynamic method (e.g., Reed and Albright 1986) is used to calculate sea surface fluxes over the Bering Sea for 1800 UTC 8 March, just after the mature arctic hurricane passed St. Paul Island. Given the steady-state nature of the mature vortex, a time to distance transformation of surface data at St. Paul Island and Cape Newenham was used to transpose data into the observation sparse vicinity. The results (Fig.
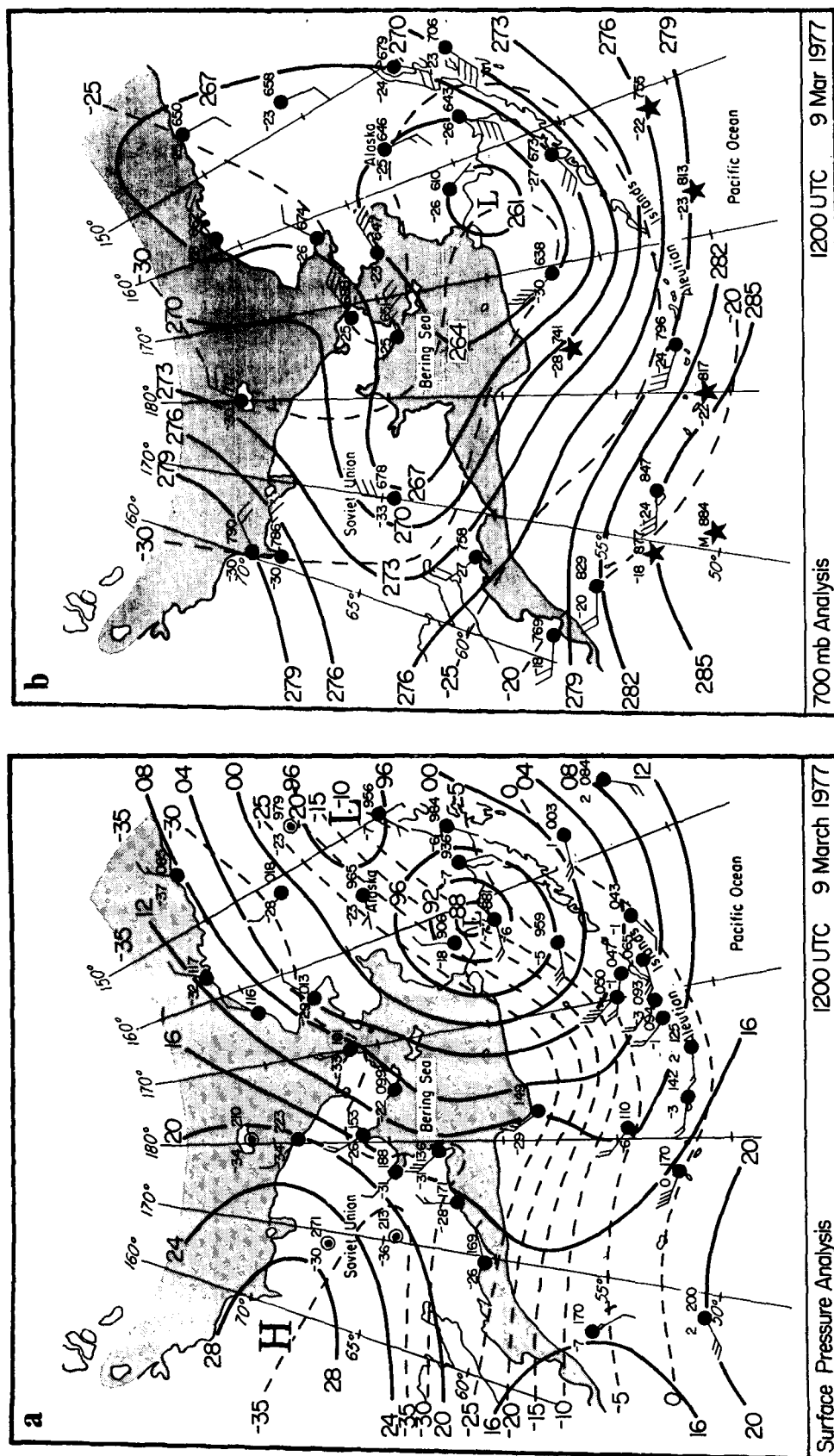
FIG. 10. As in Fig. 4, except for 1200 UTC 9 March 1977: (a) Surface-pressure analysis, (b) geopotential analysis for 700 mb.
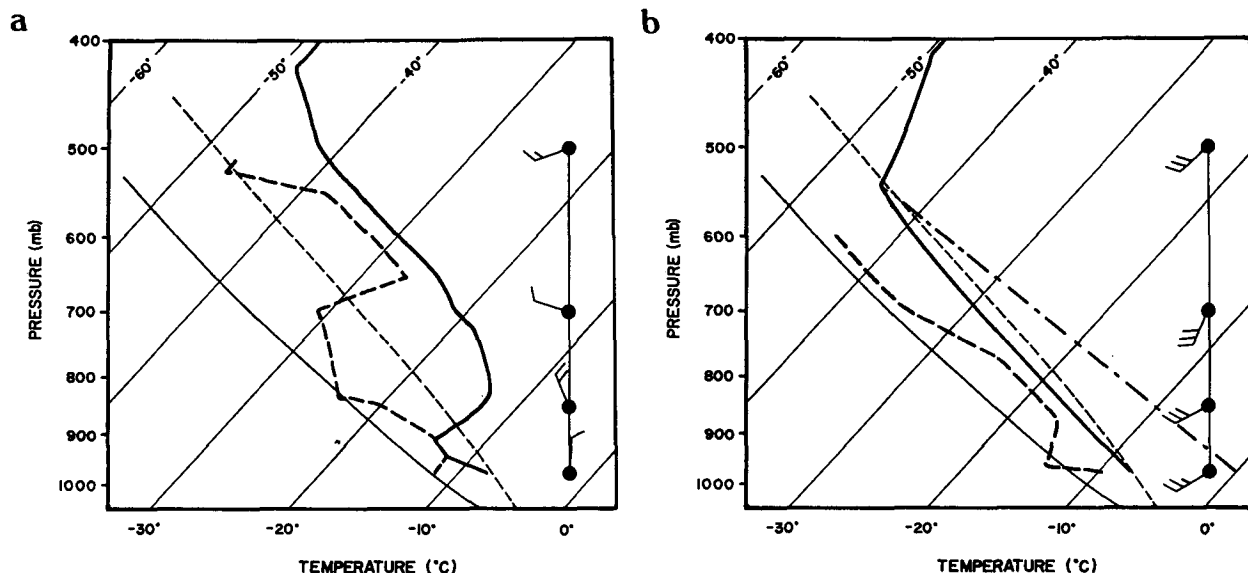
FIG. 11. Rawinsonde soundings for St. Paul Island at (a) 1200 UTC 7 March 1977, (b) 1200 UTC 8 March 1977. The temperature and dewpoint (°C) profiles are indicated by the heavy solid and dashed lines, respectively. Dry adiabats are shown as thin solid lines, moist adiabats as thin dashed lines. Winds: half barb 2.5 m s^{-1}, full barbs 5 m s^{-1}. Dot–dash line in (b) is the estimated lapse rate in the core of the arctic hurricane (refer to section 4).

14) show a maximum sensible heat flux (>300 W m^{-2}) in a tongue of arctic air just to the west of the surface-low center. Sensible heat fluxes drop to less than 50 W m^{-2} at the core of the low in response to relatively warm surface air temperatures and light winds observed at St. Paul Island at this time.

To further explore the relationship of the surface heating and the arctic hurricane, we utilize a quantity designated "potential thickness" (Davis and Emanuel 1988), defined as the thickness that would result if the environmental lapse rate were modified to lie along a moist adiabat representing saturation at 1000 mb and at the sea surface temperature. Conceptually the potential thickness represents an upper limit to which sea surface fluxes can modify the atmosphere. Davis and Emanuel (1988) have shown empirically that potential thickness depends only on the sea surface temperature. Figure 15 shows the difference in meters between the potential thickness, computed using the sea surface temperatures in the Bering Sea (Fig. 3), and the actual environmental thickness for 1200 UTC 8 March. A maximum > 380 m between the potential thickness and the environmental thickness occurs at the location of the surface low at this time. Calculations for 0000 UTC 8 March show the same relationship (not shown). This result is consistent with the observed phasing of the motion of the mature arctic hurricane and that of the upper-level vortex and is suggestive of a link between the ability of the sea surface fluxes to modify the atmosphere and the location of the surface low.

The St. Paul Island sounding for 1200 UTC 8 March (Fig. 11b) was taken less than 6 h prior to the arctic

hurricane passage. A sounding of the atmosphere near the core of the arctic hurricane can be constructed with information from the 1200 UTC sounding, and surface observations at St. Paul Island. First the mean virtual temperature of the core sounding is calculated using a form of the hypsometric equation (Wallace and Hobbs 1977):

$$ \overline{T_v} = \left[\ln\left(\frac{p_s}{p_z}\right) \right]^{-1} \left(\frac{g_0 Z}{R}\right), \qquad (3) $$

where $\overline{T_v}$ = mean virtual temperature of the atmosphere in the layer from the surface to 500 mb, p_s = sea-level pressure (estimated at ∼970 mb), p_z = 500 mb, Z = 500-mb geopotential height (4870 m at 1200 UTC), g_0 = gravitational acceleration, and R as in Eq. (2).

After substitution a result of 251 K is obtained for $\overline{T_v}$. The lapse rate of the core sounding can then be determined graphically (Fig. 11b) by anchoring the sounding with a 500-mb temperature (assumed to be ∼ −46°C), using the mean virtual temperature and a constant lapse rate. The resulting lapse rate of ∼9°C km^{-1} is nearly dry adiabatic. A surface temperature of ∼0°C is determined from the core sounding. A maximum surface temperature of −3°C was observed at St. Paul Island at 0644 LST 8 March, near the core of the arctic hurricane.

In an extension to the steady-state theory of Emanuel (1986), ER pointed out that the arctic hurricane, like its tropical counterpart, may be regarded as a natural example of a Carnot heat engine. By integrating the

Bernoulli equation around a closed circuit in a steady-state arctic hurricane, an exact equation for the maximum pressure drop along the surface from the outermost closed isobar to the storm center can be derived (for details of the derivation the reader is referred to Emanuel and Rotunno 1989):

$$\ln \frac{p_a}{p_c} = 3.5 \left(\frac{\overline{T_s} - \overline{T_0}}{\overline{T_s}} \right) \ln \frac{\theta_{ec}}{\theta_{ea}}. \tag{4}$$

From the surface observations at St. Paul Island (Fig. 2), $\theta_{ec} = 278.5$ K, $\theta_{ea} = 270.6$ K, and $\overline{T_s} = 266$ K. From the surface analysis at 1800 UTC 8 March (Fig. 8c), $p_a = 988$ mb, and from the proximity sounding at 1200 UTC 8 March, $\overline{T_0} \sim -45°C = 228$ K. When these values are substituted into the preceding equation, $p_c = 973$ mb. This value agrees well with the observed central pressure (Fig. 8c). As in the case investigated by ER, the potential for further development exists since theoretically θ_{ec} could approach a value that represents saturation at the sea surface temperature ($\sim 2°C$).

5. Polar-low simulations with an axisymmetric model

The analyses described in the previous sections suggest that the arctic hurricane initially developed in response to a combination of low-level baroclinicity and cyclonic vorticity, produced by differential surface heat fluxes, and synoptic-scale forcing associated with a short-wave trough aloft. In its mature stage the storm maintained its strength and a symmetric cloud structure (in the absence of significant quasi-geostrophic forcing) until landfall after which it rapidly dissipated. It is clear from the surface analyses and the time series station data from St. Paul Island presented in section 2 that low-level baroclinicity was present to some degree in the vicinity of the low center. However, it is not clear what role this baroclinicity played in the final structure and energetics of the arctic hurricane. In this section, we will employ an axisymmetric numerical model to demonstrate that, given that a disturbance of sufficient amplitude exists, an arctic hurricane can develop in an environment similar to that documented in this paper by a vortex–ocean interaction that taps a large reservoir of energy at the ocean surface. In this regard, our spirit is the same as ER's. The use of axisymmetric geometry eliminates baroclinic instability as mechanism to sustain the polar low.

a. Description of the numerical model

The numerical model used in this study is based on the axisymmetric tropical cyclone model described by Baik et al. (1990). Therefore, only a brief summary, some modifications made, and a changed cumulus convective parameterization are presented here. The model contains the conservation equations for momentum, mass, energy, and water vapor. Hydrostatic balance is assumed in the vertical momentum equa-

tion. The system of governing equations is derived on an f plane with axisymmetric polar coordinates in the horizontal and σ coordinate in the vertical. The σ coordinate is defined by $\sigma \equiv (p - p_T)(p_s - p_T)^{-1}$, where p_T is the pressure at the model top (specified as 100 mb for the present study) and p_s the surface pressure. The model atmosphere has 15 vertical layers with uniform grid spacing and an equally spaced horizontal resolution of 20 km on a horizontal domain size of 1500 km. The Orlanski (1976) radiation condition is employed to minimize gravity wave reflections at the lateral boundary. This boundary condition is applied vertical level by vertical level. The spectral radiation boundary condition implemented in the tropical cyclone model (Baik et al. 1990) was applied vertical mode by vertical mode. The governing equations are solved numerically using the finite-difference method. The time step is 30 s.

The model includes subgrid-scale horizontal and vertical diffusion, bulk aerodynamic calculations of surface momentum, heat, and water vapor, radiation, grid-scale phase change, dry convective adjustment, and subgrid-scale moist convection. The radiation scheme uses Newtonian cooling (Rotunno and Emanuel 1987) given by

$$Q_R = -\frac{\theta - \theta_0}{\tau_R}, \tag{5}$$

where θ is the potential temperature, θ_0 the initial potential temperature, and τ_R the relaxation time scale for the radiational cooling. This relaxes the temperature towards the initial state. The radiation scheme is applied at every level and the τ_R is set to 12 h. In the grid-scale phase change processes, all excess liquid water resulting from supersaturation is converted into snow and immediately falls out onto the surface. Therefore, the latent heat of sublimation is used in the calculation of grid-scale phase change instead of the latent heat of evaporation.

The cumulus convective processes are parameterized using the Kuo (1974) scheme. The temperature and mixing ratio inside the cloud are taken along a moist adiabat constructed using a saturation point at the lowest model level (level 15). The moistening parameter b, the fraction of total moisture convergence that is stored in the air to increase the humidity, is computed by the method proposed by Anthes (1977a), which is expressed by

$$b = \left(\frac{1 - \langle RH_e \rangle}{1 - RH_c} \right)^n \quad \text{if} \quad \langle RH_e \rangle \geq RH_c$$

$$b = 1 \qquad\qquad \text{if} \quad \langle RH_e \rangle < RH_c. \tag{6}$$

Here $\langle RH_e \rangle$ is the mean environmental relative humidity in the air column, RH_c a threshold relative humidity, and n a positive exponent. Only environmental moistening occurs when $\langle RH_e \rangle$ is less than RH_c. The
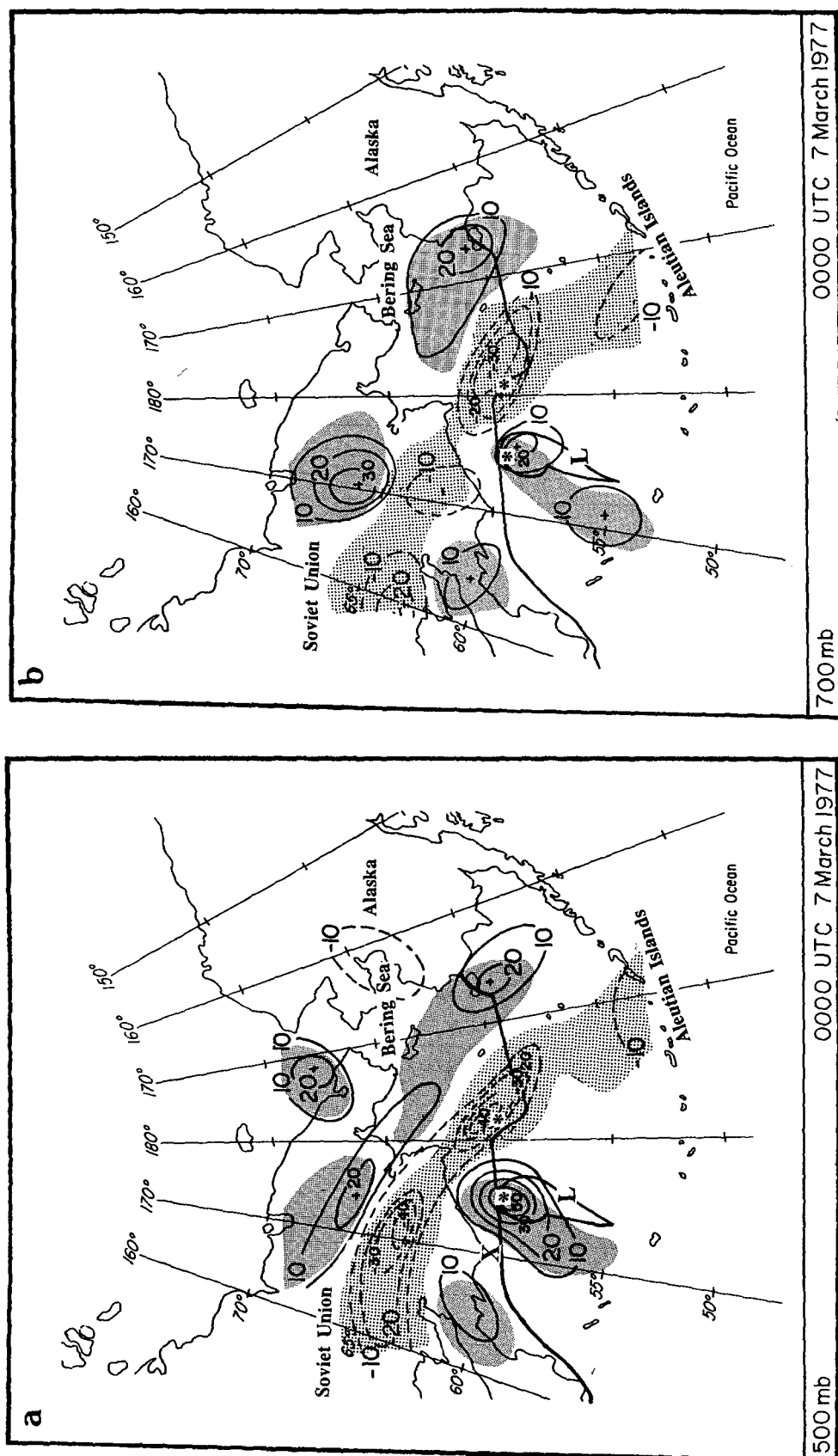
FIG. 12. Convergence of $\mathbf{Q}$ ($-2\nabla \cdot \mathbf{Q}$, contours every 10×10^{-5}) at 0000 UTC 7 March for (a) 500 mb, (b) 700 mb, and (c) 850 mb. Solid contours indicate upward forcing, and the dashed contours indicate downward forcing. The "L" indicates the surface-low position at this time, and the "X" in (a) indicates the location of the cyclonic vorticity maximum at 500 mb. The fine shading indicates regions of $\omega \leqslant -1\ \mu b\ s^{-1}$. The coarse shading indicates regions of $\omega \geqslant 1\ \mu b\ s^{-1}$. Asterisks indicate the locations of the maximum and minimum values of ω. For reference the location of the comma cloud and ice edge are indicated by the heavy lines.
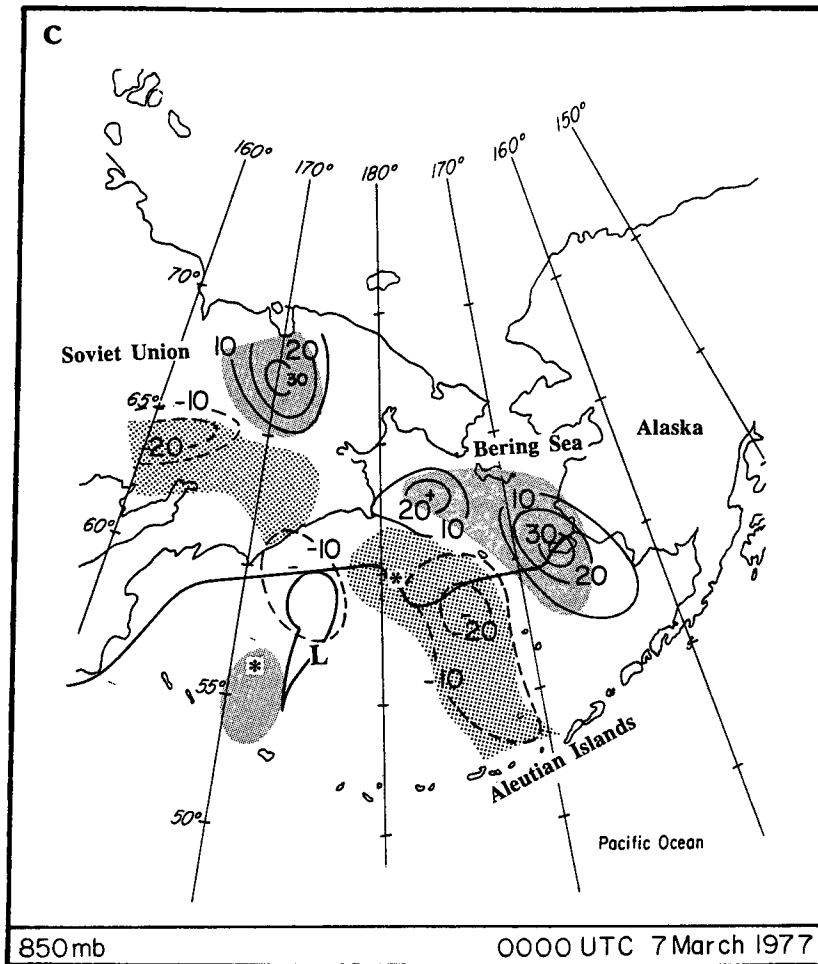
FIG. 12. (*Continued*)

RH_c and n are specified as 0.5 and 3 for this study. Deep cumulus convective processes are activated in a conditionally unstable atmosphere when the vertically integrated moisture convergence rate exceeds a critical value of 10^{-5} kg m^{-2} s^{-1}, with the computed cloud-top height being above level 12.

The initial tangential wind field is given by

$$v = v_m \left[\frac{2(r/r_m)}{1 + (r/r_m)^2} \right] \left[\frac{3(\sigma/\sigma_m)}{2 + (\sigma/\sigma_m)^3} \right], \qquad (7)$$

where v is the tangential wind speed, v_m the maximum tangential wind speed, and r the radius in polar coordinates. The radius of the maximum wind r_m and the σ level of the maximum wind σ_m are specified as 50 km and 0.9, respectively. Zero radial wind is assumed initially. An average of the 1200 UTC 7 March and 1200 UTC 8 March soundings at St. Paul Island (Fig. 11) is used as the initial temperature state at the model lateral boundary. The initial surface pressure at the lateral boundary is set to 1005 mb. The temperature and pressure distributions inside the lateral boundary ($r = 1500$ km) are determined using the hydrostatic

and gradient-wind equations. For the initial moisture field the relative humidity is assumed to decrease linearly with height (with respect to σ coordinate) with relative humidities of 80%, 70%, and 10% at levels 15, 10, and 1, respectively. A Gaussian-type perturbation with 15% amplitude in relative humidity and e-folding radius of 100 km centered at 40-km radius from the model center is added to the initial moisture field to enhance the storm development. The Coriolis parameter is evaluated at 57.3°N (latitude of St. Paul Island). For control simulation, v_m is specified as 10 m s^{-1} and the sea surface temperature is set to 2°C. These values are close to those observed (see Figs. 3 and 4). The initialization procedure for the control simulation gives a minimum surface pressure of 996.8 mb at the center. Insofar as the model results are closely related to the initial field, comparisons of the model results and the observations in the next subsection are qualitative.

b. Model results and discussion

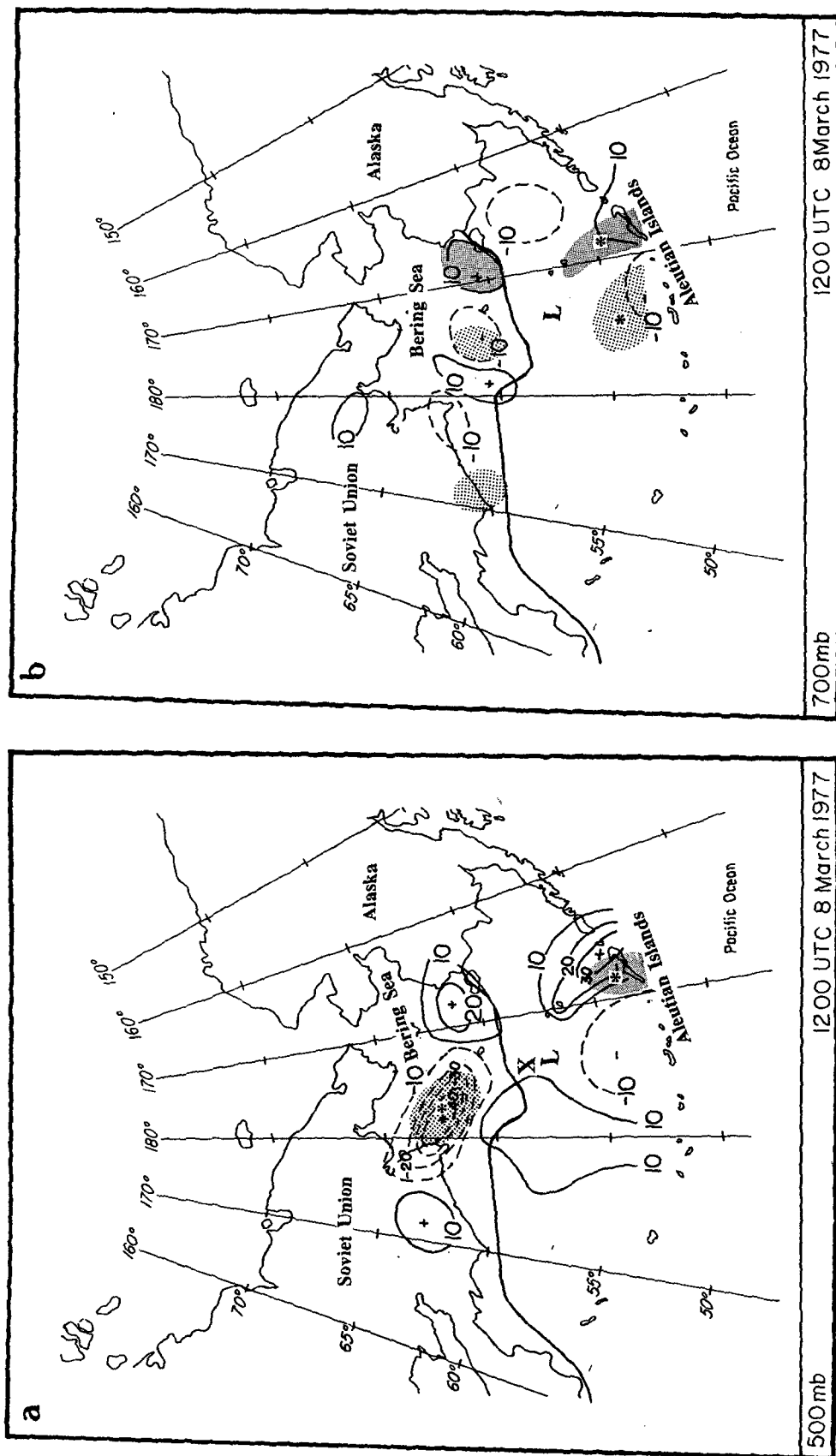Figure 16 shows the time evolution of the minimum surface pressure and maximum tangential wind speed

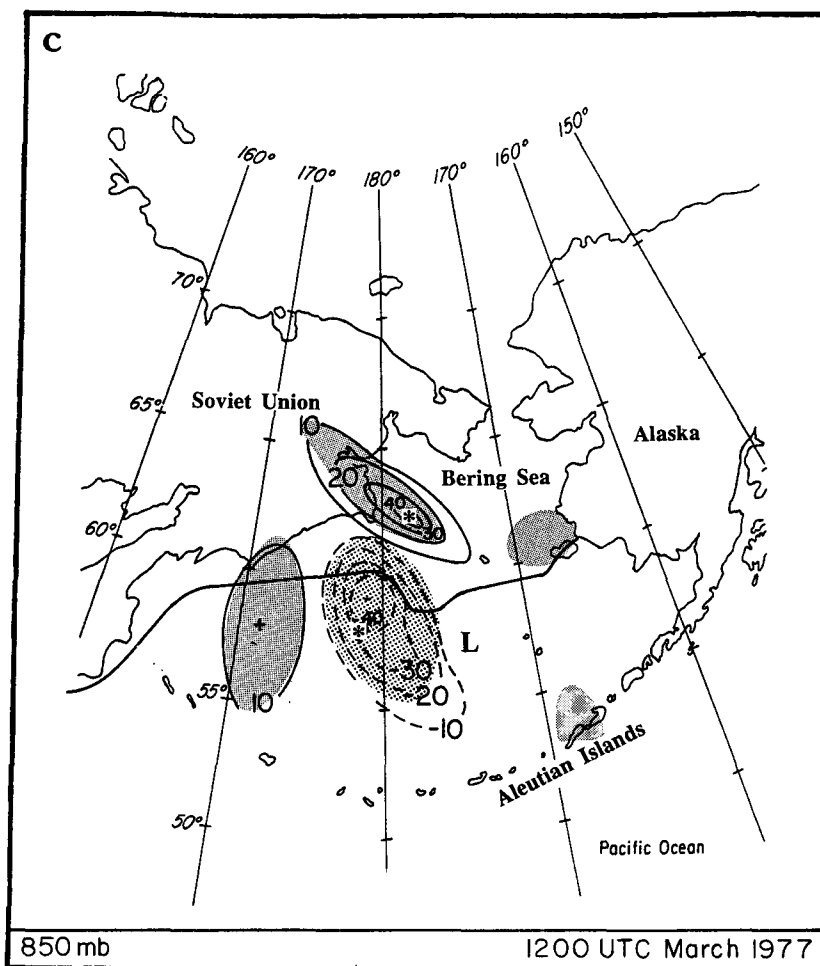FIG. 13. As in Fig. 12, except for 1200 UTC 8 March.

FIG. 13. (Continued)

for the control simulation. This figure indicates that the development of a polar low can be simulated with sea surface energy supplied by a vortex–ocean interaction in the absence of synoptic-scale baroclinicity. The model storm experiences a weakening stage during the first 6 h because of the destruction of the initial gradient-wind balance by sudden introduction of surface friction (Anthes 1977b) and then intensifies gradually. After ~54 h, the storm is in a quasi-steady state (mature stage). At the mature stage, the minimum surface pressure and maximum tangential wind speed are about 970 mb and 27 m s^{-1}. It takes a longer time period for the model storm to develop a mature storm (~36 h) than is suggested by observation (~24 h). However, the predicted final storm intensity in terms of the minimum surface pressure and wind speed agrees very well with the observations (central pressure of ~970 mb in Fig. 8c) and the analytical result (~973 mb), suggesting that sea surface fluxes played a major role in the evolution and maintenance of the St. Paul arctic hurricane.

Although the simulated and observed minimum surface pressures are very similar to each other, it is difficult to unambiguously choose the value of the initial ambient pressure from the observations, because of the large surface pressure gradients present in the vicinity of the polar low. Therefore, a pressure perturbation field might provide a better comparison. A central surface pressure at the very early stage of the polar low is unknown due to the lack of observations. If we assume an initial central surface pressure of 990 mb, the surface pressure difference at the storm center between the initial stage and mature stage is around 20 mb. In the numerical model, the surface pressure difference is 27 mb.

The time variations of the sensible, latent, and total (sensible plus latent) heat fluxes at the surface at 100-km radius are shown in Fig. 17. The sensible and latent heat fluxes decrease during the first ~16 h and gradually increase until the model storm achieves a steady state. The decrease in the surface heat fluxes during the early stage is related to the weakening of the model
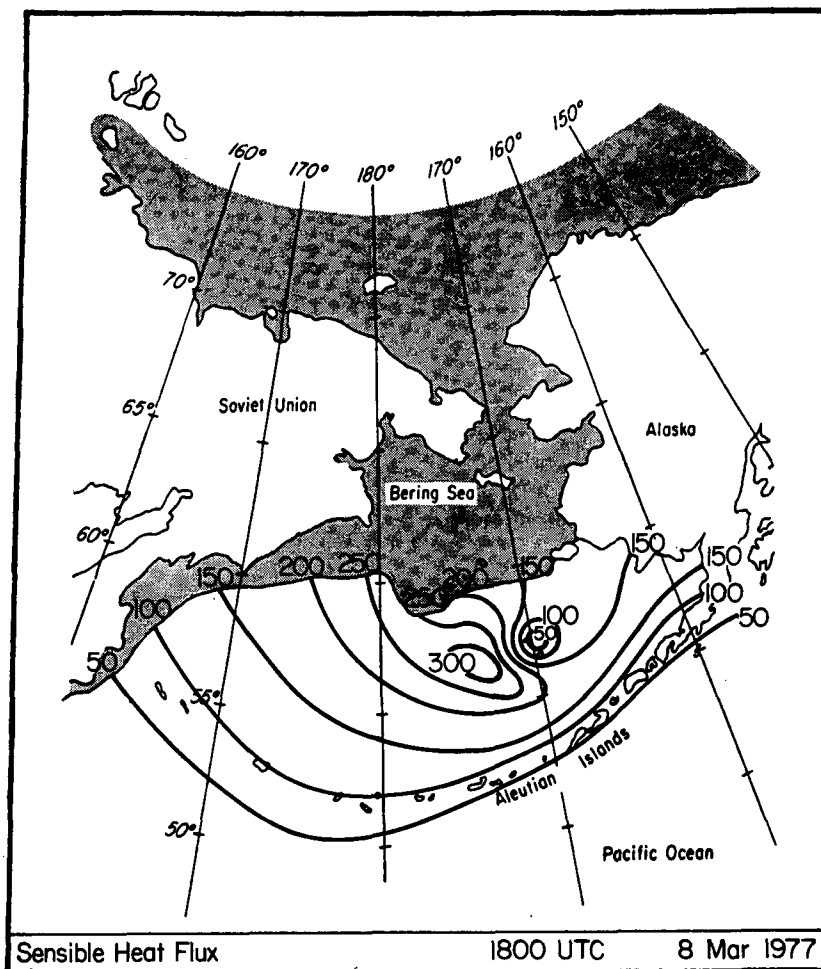
FIG. 14. Sensible heat flux (solid contours every 50 W m^{-2}) at 1800 UTC 8 March.

storm, and the subsequent decrease is partly associated with the gradual outward shift of the radius of maximum wind from 100 km. However, as the storm develops, the radius of the maximum wind moves inwards. Figure 17 also shows that the sensible heat flux is greater than the latent heat flux during the entire time period of the simulation. The computed sensible and latent heat fluxes at the mature stage are ~310 and ~250 W m^{-2}, respectively, giving a total surface heat flux of ~560 W m^{-2} and a Bowen ratio of 1.24. The maximum sensible heat flux agrees well with that calculated from the observational data (Fig. 14).

In order to investigate the structure of subgrid-scale latent heating produced by the Kuo convective parameterization at the mature stage, the vertical convective heating profiles at radii where active convective processes take place at 72 h are shown in Fig. 18. The overall shape of the heating profiles, with maxima located near or below the midtroposphere, are similar to the normalized convective heating profiles constructed using the actual thermodynamic soundings of polar

lows (Sardie and Warner 1985). The convective heating profiles at 80- and 100-km radii are similar to each other, and the heating rate there is greater than that at 60-km radius. The maximum convective heating rate at 100-km radius occurs at the σ coordinate of 0.77, and its value is about 55°C day^{-1}.

To examine the latent heating partition in the arctic hurricane simulation, the time variation of the ratio of the inner 300-km-domain-averaged convective-to-total (convective plus grid-scale) precipitation rate is shown in Fig. 19. Recall that in this study all precipitation is in the form of snow. The time evolution of the ratio is very different from that seen in the tropical cyclone simulations (Baik et al. 1990).

Analyses of the simulated precipitation rates from the axisymmetric tropical cyclone model with a horizontal resolution of 20 km indicate that the latent heat release comes mainly from the grid-scale phase change during the rapidly intensifying and mature stages of the tropical cyclone. This result is true regardless of whether the Betts or the Kuo convective scheme is used
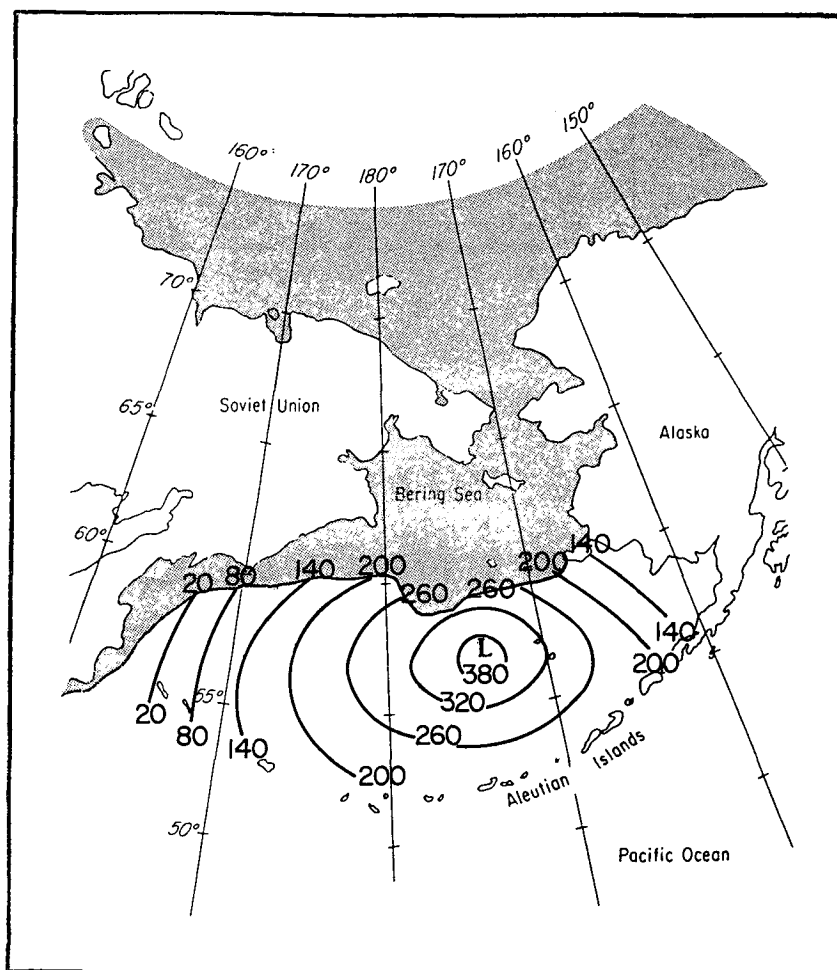
FIG. 15. Difference between the potential thickness (see text) and the environmental thickness in meters for 1200 UTC 8 March, computed using the sea surface temperatures in the Bering Sea (Fig. 3). The "L" indicates the position of the surface low at this time (see Fig. 8b).

to parameterize the convective processes in the model (Baik et al. 1991).

In the simulation of the arctic hurricane, the grid-scale precipitation starts shortly after the time integration begins, while the subgrid-scale convective precipitation starts at the 6-h time step (Fig. 19). Therefore, the ratio is zero during the first 5 h. Thereafter, the ratio is between 0.46 and 0.59 until the end of the time integration. This means that, within the context of the present model simulation, the subgrid-scale latent heating is comparable to the grid-scale latent heating during the development and maintenance of the arctic hurricane.

The results from the axisymmetric tropical cyclone and arctic hurricane simulations imply that the partition of the latent heating into the grid scale and subgrid scale in the numerical model depends on the characteristics of the atmospheric environment even if the same horizontal resolution and cumulus parameterization are used. The storm intensity in the tropical

cyclone simulation is much greater than that in the arctic hurricane simulation. Therefore, the larger fraction of grid-scale latent heating during the rapidly intensifying and mature stages of the simulated tropical cyclone is associated with stabilization of the model atmosphere by very strong latent heating at mid- and upper levels that removes convectively unstable layers. On the other hand, the latent heating in the arctic hurricane simulation is not strong enough to stabilize the model atmosphere, in the presence of a larger sensible heat flux at the surface.

Figure 20 shows the thermodynamic structure of the mature arctic hurricane at 72 h. For increased resolution, only the radius–height cross sections of the inner 500-km domain are shown in these figures. The temperature deviation field from the model lateral boundary (Fig. 20a) exhibits a warm region at midlevels near the center. Another warm region is seen near the surface, which is present because of the strong upward sensible heat flux from the sea surface. The relative
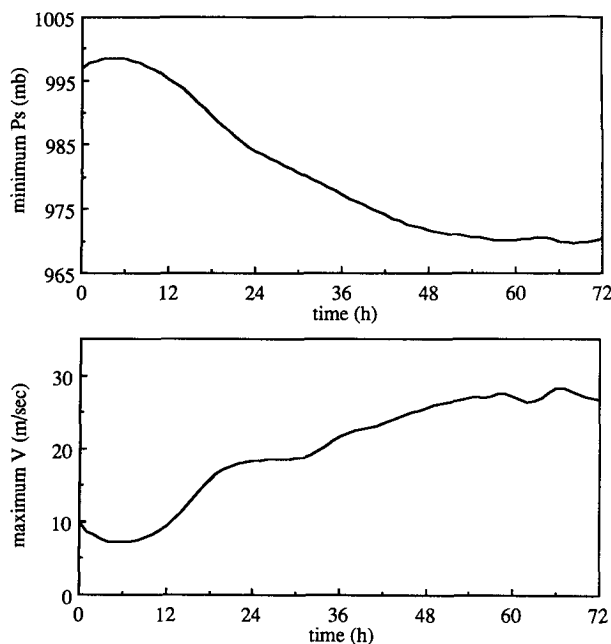
FIG. 16. The time evolution of the minimum surface pressure (upper panel) and maximum tangential wind speed (lower panel) for the control simulation.

FIG. 18. The vertical convective heating profiles at selected radii at 72 h for the control simulation.

humidity field is characterized by a moist region related to a strong updraft and the outflow (Fig. 20b). A dry region exists near the storm center, and second dry region occurs below the outflow and above $\sigma \sim 0.2$. The thermodynamic and dynamic structures (not shown) are very similar to those observed in tropical cyclones, except that the circulation of the arctic hurricane is shallower and a warm region, resulting from the sensible heat flux, exists near the surface. These results are consistent with those of ER.

Mesoscale observations above the surface are not available for this case, limiting the comparison with the model simulated structure. The diameter of the cirrus outflow in the model (~ 600 km in Fig. 20b) is

larger than satellite imagery suggests just prior to landfall (Fig. 1c), but is not inconsistent with that observed earlier (Fig. 1b).

The sensitivity of the storm development to the initial vortex amplitude was investigated by setting v_m = 2, 5, and 10 (control simulation) m s^{-1}. Time evolution of the maximum tangential wind speed for each simulation is shown in Fig. 21. The initial vortex with $v_m = 5$ m s^{-1} develops, but the final tangential wind speed is only ~ 12 m s^{-1}. The case with $v_m = 2$ m s^{-1} does not show any development except a slight disturbance growth near the end of the time integration,
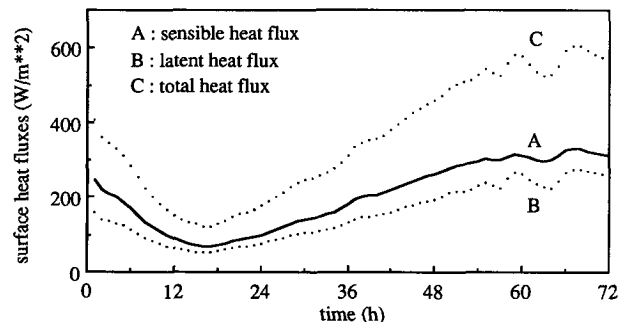

FIG. 17. The time evolution of the sensible, latent, and total heat fluxes at the surface at a radius of 100 km from the model center for the control simulation.
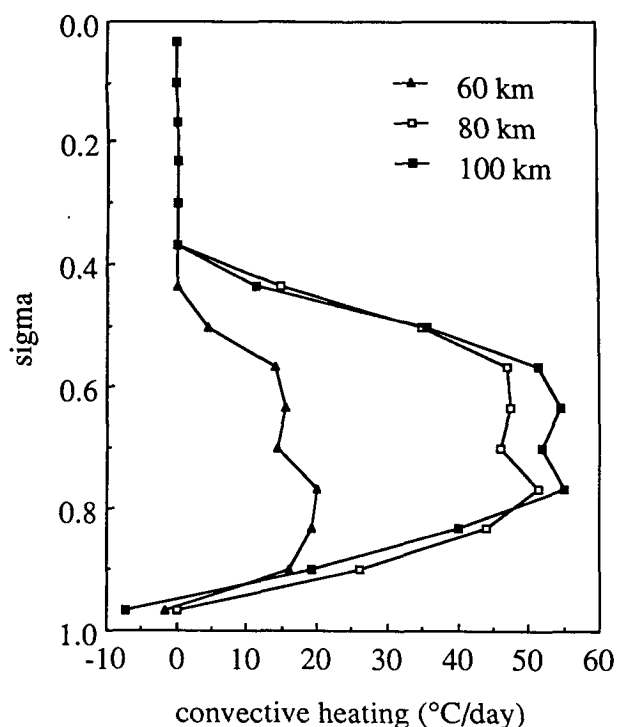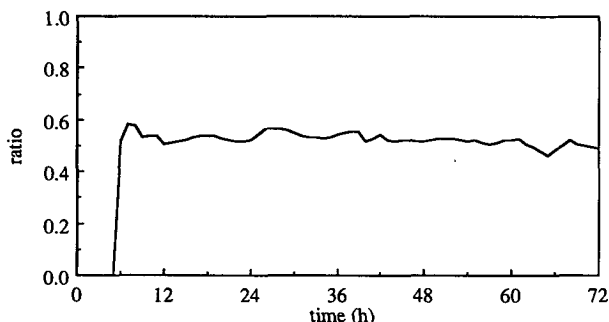

FIG. 19. The time evolution of the ratio of the inner 300-km–domain-averaged convective-to-total precipitation rate for the control simulation.
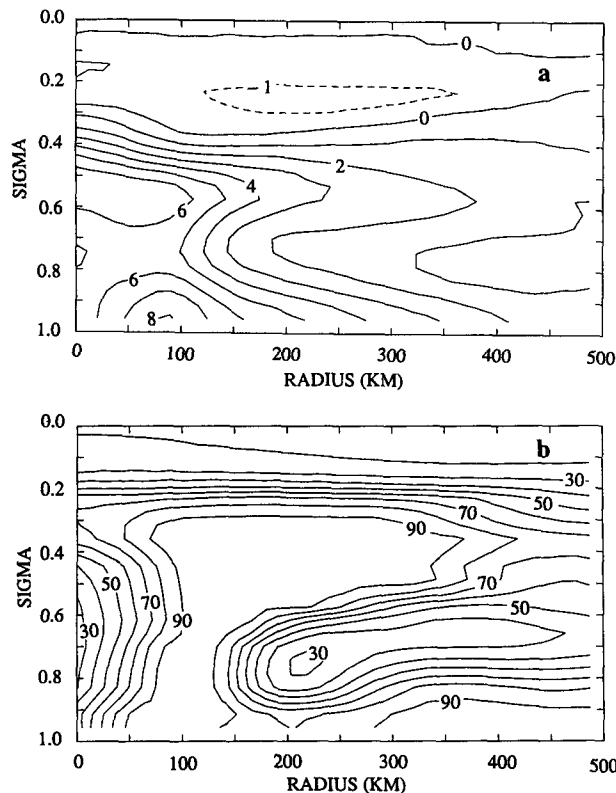
FIG. 20. The radius–height cross sections of (a) temperature deviation from the model lateral boundary (contour interval of 1°C) and (b) relative humidity (contour interval of 10%) at 72 h for the control simulation.

which occurs far away from the center at a radius of about 1170 km. These results support the idea (ER) that a disturbance with sufficient amplitude is needed to initiate intensification by a vortex–ocean interaction.

To examine the sensitivity of model storm evolution to sea surface temperature, experiments with sea surface temperatures of 0°, 2° (control simulation), and 4°C are performed. Figure 22 shows the time variation of the maximum tangential wind speed for each of these
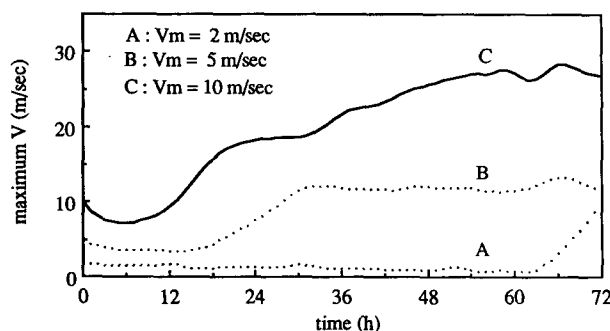

FIG. 21. The time evolution of the maximum tangential wind speed for initial vortex amplitudes of 2, 5, and 10 m s⁻¹.
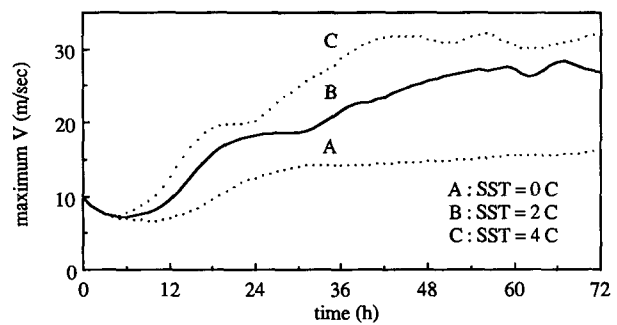

FIG. 22. The time evolution of the maximum tangential wind speed for sea surface temperatures of 0°, 2°, and 4°C.

cases. As expected, the storm experiences more rapid development and attains a more intense final stage as the sea surface temperature increases. The greater storm intensities attained by the arctic hurricane simulations described in ER are due in part to higher sea surface temperatures (7°C) representative of the Norwegian Sea.

A main difference between ER's model and the present model lies in the representation of cumulus convection. They resolve convection explicitly with a horizontal resolution of 10 km, in a nonhydrostatic framework, utilizing a prognostic equation for liquid water. In contrast, we parameterize convection with the hydrostatic assumption, and a 20-km horizontal resolution. The initial vortex structures for the two control simulations are similar to each other, but the initial thermodynamic profiles and sea surface temperatures are different from each other. Emanuel and Rotunno employed a thermodynamic sounding (with some low-level modifications) taken on Bear Island at 1200 UTC 13 December 1982, near the northern edge of a polar low that occurred over the Norwegian Sea. The sea surface temperature was specified at 7°C. In spite of these differences, both model results support the hypothesis that a polar low can be maintained solely through an air–sea interaction instability mechanism.

Although the present case study confirms the importance of sea surface energy fluxes, it is not clear to what extent air–sea interaction instability operated relative to baroclinic instability in the documented arctic hurricane. Numerical experiments with a 3D mesoscale model in which sea surface fluxes are alternately turned on and off could help clarify the relative importance of the air–sea interaction process for this interesting case.

6. Summary and conclusions

In early March 1977 a mesoscale polar low developed over the western Bering Sea and tracked eastward along a zone of large sea surface temperature gradient. Satellite imagery of the mature storm revealed spiral clouds bands of mesoscale extent (~300-km diame-

ter), with an unusual symmetry and a clear eye. The mature storm maintained its symmetric structure and strength for over 36 h, passing the rawinsonde station at St. Paul Island on 8 March. A sharp maximum in surface equivalent potential temperature was observed at St. Paul Island in the core of the low. The low rapidly dissipated after making landfall on 9 March, with winds observed in excess of 30 m s^{-1} at Cape Newenham on the west coast of Alaska. The unusual symmetry displayed by the storm's cloud shield in its long path across the Bering Sea, its thermodynamic structure, and the success of an axisymmetric numerical model in simulating major features of the storm led to adoption of the term *arctic hurricane* in this study.

Synoptic analyses reveal that the arctic hurricane formed at the leading edge of an outflow of arctic air that originated over the ice and passed over the open water of the Bering Sea. This outflow is characterized by cold advection in the lower and midtroposphere, with strong surface fluxes of latent and sensible heat into the boundary layer from the underlying sea surface. Recent observational studies have shown that this type of outflow leads to destabilization of the troposphere, and the development of low-level baroclinicity and cyclonic vorticity (e.g., Businger and Reed 1989b).

Aloft a large cold-core low dominated the Bering Sea region. The incipient storm formed when a well-defined short-wave trough in the mid- and upper troposphere crossed the Siberian coast at 0000 UTC 7 March 1977. Quasi-geostrophic analysis shows a maximum in ascending motion aloft ($\omega \sim -4 \mu$b s^{-1}) over the head of a comma cloud that is associated with the incipient low. This suggests that the initial development of the disturbance was induced by a cyclonic potential-vorticity anomaly in the upper troposphere, associated with the upper-level short wave, that acts on vorticity-rich air at low levels (Hoskins et al. 1985).

Satellite imagery and ship observations reveal a mature vortex at 0000 UTC 8 March. At this stage the low center was located beneath the cyclonic vorticity maximum aloft, and tracked with the upper-level low. Analysis of quasi-geostrophic forcing during its mature stage indicates that the forcing was minimal at all levels near the surface-low position. However, synoptic-scale descent is implied in the lower troposphere in a region of cold advection to the west of the low.

Rawinsonde data from St. Paul Island show significant cooling in the layer from ~880 to 500 mb during the 24-h period preceding the polar-low passage, while temperatures below ~880 mb warm, greatly decreasing the static stability of the troposphere. Thermodynamic calculations suggest that the surface latent and sensible heat fluxes played a significant role in the sustenance of the mature arctic hurricane. The location of the arctic hurricane coincided with the region where sea surface fluxes had the maximum potential to modify the troposphere. This region moved eastward in phase with the eastward progression of the cold-core

low aloft, as did the storm. In addition, an analytical calculation of the pressure drop from the outermost closed isobar to the storm center based on the Carnot cycle (Emanuel and Rotunno 1989) results in a central pressure of 973 mb, which agrees well with observation.

An axisymmetric numerical model with the Kuo (1974) cumulus parameterization scheme, previously used to simulate tropical cyclone development, was employed to investigate the ability of the air–sea interaction instability to sustain the arctic hurricane in the absence of baroclinic instability. The initial environment for the model integration was set to be similar to that observed with the St. Paul Island arctic hurricane.

The model correctly predicts the minimum sea-level pressure and the strength of the wind circulation attained by the storm. Also, the predicted maximum sensible heat flux agrees well with that calculated from the observational data. These results confirm that some polar lows can develop and be maintained primarily through a sea surface energy supply tapped by a vortex–ocean interaction. The dynamic and thermodynamic structures of the simulated mature storm are very similar to those of tropical cyclones except that the circulation of the arctic hurricane is shallower and a warm region exists near the surface due to the strong upward sensible heat flux from the sea. In contrast to the results for tropical cyclone simulations (Baik et al. 1991), the subgrid-scale latent heating is found to be comparable to the grid-scale latent heating during the development and maintenance of the storm. This indicates that the latent heating in the simulated arctic hurricane is not sufficient to remove convectively unstable layers, in the presence of a larger sensible heat flux at the surface.

Sensitivity studies of the initial vortex amplitude indicate that a preexisting disturbance of adequate amplitude is needed to initiate intensification by a vortex–ocean interaction. The model storm experiences more rapid development and attains a more intense final stage as the sea surface temperature is increased.

The predicted time for development (~36 h), with a sea surface temperature of 2°C, is longer than the observations suggest, and the diameter of the simulated anvil outflow is somewhat larger than satellite imagery indicates. This points to the likely importance of other physical mechanisms, such as baroclinic instability, especially in the early stage of the evolution of the St. Paul Island storm.

The numerical model employed in this research provides only a rough approximation to the actual three-dimensional environment in which the arctic hurricane formed. The impact of the low-level baroclinicity, present throughout this storm's history, on the structure and maintenance of the disturbance is not accounted for in the model. The need for additional simulation experiments utilizing a three-dimensional, mesoscale primitive-equation model is clear, if a more complete understanding of the complex dynamics of

arctic hurricanes is to be attained. Such a model must contain realistic parameterizations of the surface transfers of heat, momentum, and moisture between the ocean and the atmospheric boundary layer, in addition to a realistic convection prescription—two notably difficult challenges in numerical modeling. The success of additional modeling efforts will also depend in large part on the availability of in situ observational data, particularly on the mesoscale, in various stages of the life cycle of an arctic hurricane.

APPENDIX

Objective Analysis Scheme and Numerical Computations

If Q represents any meteorological variable, calculations of gridpoint values are obtained by (Barnes 1964 and 1973):

$$\bar{Q} = \sum_{i=1}^{N} w_i Q_i / \sum_{i=1}^{N} w_i.$$

The interpolated gridpoint value is the weighted mean $\bar{Q}$ of observations surrounding the point. The value N is the total number of stations influencing a given grid point, w_i is the observation weight, and Q_i is the observed value. The observation weights w_i are inverse-distance d dependent and are defined by $w_i = \exp(-d^2/4k_0)$. Here k_0 is the "weight parameter" that controls the rate at which the weight value decreases outward from the point of interpolation. Hence, k_0 determines the degree of smoothing of the data field: if k_0 is small, there is little smoothing; if k_0 is large, there is greater smoothing.

The appropriate choice of k_0 can be determined by selecting the amplitude suppression (response function) of the minimally resolved wavelength, the latter being twice the average station spacing. All available rawinsonde and satellite data were utilized in the calculations. The upper-air station spacing is taken to be comparable to the United States radiosonde network

($\sim$450 km). If the minimally resolved waves are suppressed to about 16% of their initial amplitude, the two-pass Barnes theory suggests a weight parameter of about 99 000 km^2. To obtain this value a convergence parameter $\gamma = 0.3$ is used in the second pass, and the weight parameter is reduced to γk_0. The previous weighted mean is then applied to the difference in the observations and the first-pass interpolated values at stations. The amplitude response adopted in this study is consistent with those chosen in other recent applications of the Barnes scheme (Barnes 1985, 15%; Moore and Blakley 1988, 21%).

All finite-difference calculations were standard second-order centered differences. Objectively interpolated values of geopotential height and temperature were obtained over a 15 × 19 grid centered at 61.5°N, 176°W over the Bering Sea. The grid spacing at the mean latitude of the grid (61.5°N) is $\sim$165 km.

REFERENCES

Anthes, R. A., 1977a: A cumulus parameterization scheme utilizing a one-dimensional cloud model. *Mon. Wea. Rev.*, **105**, 270–286.

——, 1977b: Hurricane model experiments with a new cumulus parameterization scheme. *Mon. Wea. Rev.*, **105**, 287–300.

Baik, J.-J., M. DeMaria and S. Raman, 1990: Tropical cyclone simulations with the Betts convective adjustment scheme. Part I: Model description and control simulation. *Mon. Wea. Rev.*, **118**, 513–528.

——, —— and ——, 1991: Tropical cyclone simulations with the Betts convective adjustment scheme. Part III: Comparisons with the Kuo convective parameterization. *Mon. Wea. Rev.*, **119**, in press.

Barnes, S. L., 1964: A technique for maximizing details in numerical weather map analysis. *J. Appl. Meteor.*, **3**, 396–409.

——, 1973: Mesoscale objective analysis using weighted time-series observations. NOAA Tech. Memo. ERL NSSL-62, Norman, OK, 60 pp.

——, 1985: Omega diagnostics as a supplement to LFM/MOS guidance in weakly forced convective situations. *Mon. Wea. Rev.*, **113**, 2122–2141.

Bergeron, T., 1954: Reviews of tropical hurricanes. *Quart. J. Roy. Meteor. Soc.*, **80**, 131–164.

Betts, A. K., 1982: Saturation point analysis of moist convective overturning. *J. Atmos. Sci.*, **39**, 1484–1505.

Bjerknes, J., and H. Solberg, 1922: Life cycles of cyclones and the polar front theory of atmospheric circulations. *Geofys Publ.*, **3**, 1–18.

Bosart, L. F., 1981: The President's Day snowstorm of 18–19 February 1979: A subsynoptic-scale event. *Mon. Wea. Rev.*, **109**, 1542–1566.

Bratseth, A. M., 1985: A note on CISK in polar air masses. *Tellus*, **37A**, 403–406.

Brown, R. A., 1980: Longitudinal instabilities and secondary flows in the planetary boundary layer: A review. *Rev. Geophys. Space Phys.*, **18**, 683–697.

Businger, S., 1985: The synoptic climatology of polar low outbreaks. *Tellus*, **37A**, 419–432.

——, 1987: The synoptic climatology of polar low outbreaks over the Northern Pacific Ocean. *Tellus*, **39A**, 307–325.

——, and R. J. Reed, 1989a: Cyclogenesis in cold air masses. *Wea. Forecasting*, **2**, 133–156.

——, and R. J. Reed, 1989b: Polar lows. *Polar and Arctic Lows*, Twitchell, P. F., E. A. Rasmussen and K. L. Davidson, Eds., A. Deepack Publishing, 3–45.

——, and B. Walter, 1988: Comma cloud development and associated rapid cyclogenesis over the Gulf of Alaska: A case study using aircraft and operational data. *Mon. Wea. Rev.,* **116,** 1103–1123.

Charney, J. G., and A. Eliassen, 1964: On the growth of hurricane depression. *J. Atmos. Sci.,* **21,** 68–75.

Davis, C. A., and K. A. Emanuel, 1988: Observational evidence for the influence of surface heat fluxes on rapid maritime cyclogenesis. *Mon. Wea. Rev.,* **116,** 2649–2659.

Duncan, C. N., 1977: A numerical investigation of polar lows. *Quart. J. Roy. Meteor. Soc.,* **103,** 255–268.

Emanuel, K. A., 1986: An air–sea interaction theory for tropical cyclones. Part I: Steady-state maintenance. *J. Atmos. Sci.,* **43,** 585–604.

——, and R. Rotunno, 1989: Polar lows as arctic hurricanes. *Tellus,* **41A,** 1–17.

Ernst, J. A., and M. Matson, 1983: A Mediterranean tropical storm? *Weather,* **38,** 332–337.

Gyakum, J. R., and E. S. Baker, 1988: A case study of explosive subsynoptic-scale cyclogenesis. *Mon. Wea. Rev.,* **116,** 2225–2253.

Harrold, T. W., and K. A. Browning, 1969: The polar low as a baroclinic disturbance. *Quart. J. Roy. Meteor. Soc.,* **95,** 710–723.

Holton, J. R., 1979: *An Introduction to Dynamic Meteorology,* Academic Press, 391 pp.

Hoskins, B. J., I. Draghici and H. C. Davies, 1978: A new look at the omega-equation. *Quart. J. Roy. Meteor. Soc.,* **104,** 31–38.

——, and M. A. Pedder, 1980: The diagnosis of middle latitude synoptic development. *Quart. J. Roy. Meteor. Soc.,* **106,** 707–720.

——, M. E. McIntyre and A. W. Robertson, 1985: On the use and significance of isentropic potential vorticity maps. *Quart. J. Roy. Meteor. Soc.,* **111,** 877–946.

Ingraham, W. J., 1983: Temperature anomalies in the eastern Bering Sea 1953–1982. Northwest and Alaska Fisheries Center Rep. 83-21, 348 pp.

Kuettner, J. P., 1959: The band structure of the atmosphere. *Tellus,* **11,** 267–294.

Kuo, H. L., 1974: Further studies of the parameterization of the influence of cumulus convection on large-scale flow. *J. Atmos. Sci.,* **31,** 1232–1240.

LeMone, M. A., 1973: The structure and dynamics of horizontal roll vortices in the planetary boundary layer. *J. Atmos. Sci.,* **30,** 1077–1091.

Lin, Y.-L., 1989: A theory of cyclogenesis forced by diabatic heating. Part I: A quasi-geostrophic approach. *J. Atmos. Sci.,* **46,** 3015–3036.

Mansfield, D. A., 1974: Polar lows: The development of baroclinic disturbances in cold air outbreaks. *Quart. J. Roy. Meteor. Soc.,* **100,** 541–554.

Moore, G. W. K., and W. R. Peltier, 1989: On the development of polar low wavetrains. *Polar and Arctic Lows,* Twitchell, P. F., E. A. Rasmussen and K. L. Davidson, Eds., A. Deepack Publishing, 141–154.

Moore, J. T., and P. D. Blakley, 1988: The role of frontogenetical forcing and conditional instability in the Midwest snowstorm of 30–31 January 1982. *Mon. Wea. Rev.,* **116,** 2155–2171.

Økland, H., 1977: On the intensification of small-scale cyclones formed in very cold air masses heated by the ocean. Institute Rep. Series No. 26, Institute of Geophysics, University of Oslo, Norway, 25 pp.

——, 1987: Heating by organized convection as a source of polar low intensification. *Tellus,* **39A,** 397–407.

——, 1989: On the genesis of polar lows. *Polar and Arctic Lows,* Twitchell, P. F., E. A. Rasmussen and K. L. Davidson, Eds., A. Deepack Publishing, 179–190.

Orlanski, I., 1976: A simple boundary condition for unbounded hyperbolic flows. *J. Comput. Phys.,* **21,** 251–269.

Rasmussen, E., 1979: The polar low as an extratropical CISK disturbance. *Quart. J. Roy. Meteor. Soc.,* **105,** 531–549.

——, 1981: An investigation of a polar low with a spiral cloud structure. *J. Atmos. Sci.,* **38,** 1785–1792.

——, 1983: A review of mesoscale disturbances in cold air masses. *Mesoscale Meteorology—Theories, Observations, and Models,* D. K. Lilly and T. Gal-Chen, Eds., D. Reidel Publishing Company, 247–283.

——, 1985: A case study of a polar low development over the Barents Sea. *Tellus,* **37,** 407–418.

——, 1989: A comparative study of tropical cyclones and polar lows. *Polar and Arctic Lows,* Twitchell, P. F., E. A. Rasmussen and K. L. Davidson, Eds., A. Deepack Publishing, 47–80.

——, and C. Zick, 1987: A subsynoptic vortex over the Mediterranean Sea with some resemblance to polar lows. *Tellus,* **39,** 408–425.

Reed, R. J., 1979: Cyclogenesis in polar air streams. *Mon. Wea. Rev.,* **107,** 38–52.

——, and M. D. Albright, 1986: A case study of explosive cyclogenesis in the Eastern Pacific. *Mon. Wea. Rev.,* **114,** 2297–2319.

——, and C. N. Duncan, 1987: Baroclinic instability as a mechanism for the serial development of polar lows: A case study. *Tellus,* **39,** 376–384.

Rotunno, R., and K. A. Emanuel, 1987: An air–sea interaction theory for tropical cyclones. Part II: Evolutionary study using a non-hydrostatic axisymmetric numerical model. *J. Atmos. Sci.,* **44,** 542–561.

Sardie, J. M., and T. T. Warner, 1985: A numerical study of the development mechanisms of polar lows. *Tellus,* **37,** 460–477.

Shapiro, M. A., and L. S. Fedor, 1989: A case study of an ice-edge boundary layer front and polar low development over the Norwegian and Barents Seas. *Polar and Arctic Lows,* Twitchell, P. F., E. A. Rasmussen and K. L. Davidson, Eds., A. Deepack Publishing, 257–278.

——, L. S. Fedor and T. Hampel, 1987: Research aircraft measurements within a polar low over the Norwegian Sea. *Tellus,* **37,** 272–306.

Wallace, J. M., and P. V. Hobbs, 1977: *Atmospheric Science: An Introductory Survey,* Academic Press, 417 pp.

Zick, C., 1983: Method and results of an analysis of comma cloud developments by means of vorticity fields from upper tropospheric satellite wind data. *Meteorol. Rundsch.,* **36,** 69–84.